On the dynamical behavior of filled rubbers at different temperatures: experimental characterization and constitutive modeling.

A. Delattre, S. Lejeunes, Florian Lacroix, Stéphane Méo

On the dynamical behavior of filled rubbers at different temperatures: experimental characterization and constitutive modeling.

A. Delattre[a], S. Lejeunes[b,*], F. Lacroix[c], S. Méo[c]

[a] *Airbus Helicopters, Marignane, France*
[b] *LMA, CNRS, UPR 7051, Centrale Marseille, Aix-Marseille Univ, F-13402 Marseille Cedex 20, France*
[c] *LMR, EA 2640, Université F. Rabelais de Tours, France*

Abstract

This work focuses on the characterization and the modeling of the complex dynamical behavior of a butadiene rubber filled with carbon black. This material is used in helicopter rotors and submitted to severe operating conditions. In particular the effects of the environmental temperature, of the amplitudes and frequencies of cyclic loading are studied. A new constitutive model that takes into account the Payne effect, the frequency, temperature and pre-loading dependencies is proposed. A specific material parameter fitting strategy is also introduced.

Key words: Payne effect, Filled rubber, Temperature, Viscoelasticity, Multi-axial, Preload

1. Introduction

The architecture of modern helicopter rotors is based on several critical rubber parts. These parts are designed to transmit or to damp complex loadings and a precise knowledge of their behavior is required for an accurate simulation aided design of the structure. Operating conditions of these parts can be severe: a large range of ambient temperatures (-50^oC to $+70^oC$), mechanical loadings can be multiaxial and multi-frequencies with varying amplitudes. Obviously depending on the part design, rubber materials can vary in composition (matrix and fillers) or in grade (fillers and additives ratio). Therefore to cover a wide range of applications a general constitutive modeling of filled rubbers that can take into account complex loadings with an accurate response is needed.

In this paper, a butadiene rubber filled with carbon black is considered. The mechanical properties of the present material are very closed to materials used in the aforementioned applications. As many filled-rubber materials it exhibits typical phenomena (among others):

(a) Mullins effect: a softening phenomenon that occurs when the amplitude of loading is higher than the maximum previously seen amplitude.
(b) Self heating: filled rubber exhibits a strong self heating phenomenon when they are submitted to mechanical loadings.
(c) Thermal softening: far from the glass-transition temperature, an increase of the environmental temperature leads to a dynamical softening of the material behavior. *A contrario*, regarding only the response of the rubber gum (with a very low filler ratio or for small deformation rates) an increase of temperature (far from the glass-transition) leads to a stiffening behavior which is a fundamental characteristic of the entropic elasticity behavior of rubbers. Furthermore, the competition of this entropic elasticity and the thermal dilatation leads to the well known effect of thermal inversion.

*Corresponding author
Email addresses: lejeunes@lma.cnrs-mrs.fr, tel: 033491054382,fax: 033491054749 (S. Lejeunes)

(d) Frequency dependency: when submitted to harmonic loadings with increasing frequency, the dissipated energy and the dynamical stiffness usually increase (nonlinear effect).
(e) Amplitude dependency or Payne effect: when submitted to harmonic loadings with increasing amplitude, the dissipated energy increases and the dynamical stiffness decreases (softening effect).
(f) Mean stress or static/dynamic effect: the dynamical stiffness can exhibit a nonlinear dependency on the pre-stress (preload) or mean-stress value.

In the present paper, we focus on the last four points. The Mullins effect and the self-heating phenomena are not considered for the modeling part. Concerning Mullins effect, experimental characterization has been done by applying a preconditioning to samples ("de-Mullinized"). Samples have been subjected to several initial cycles with an amplitude that was higher than the maximum amplitude used for the dynamical characterization. The self heating phenomenon or other thermo-mechanical coupling effects cannot be removed by a specific experimental procedure. These effects can be taken into account in the modeling part by a coupled thermo-mechanical approach (see for instance Reese and Govindjee (1997); Meo et al. (2002) for thermo-mechanical couplings with finite strain viscoelastic behaviors).

In the literature, many constitutive models has been proposed the last 25 years and at least three approaches can be distinguished to cover the aforementioned phenomena. The first one is the integral approach for which the viscous stress is described as a function of the whole history of strain (see for instance Coleman and Noll (1961); Morman (1988)). This approach can be used in the frequency or the time domain and gives generally very good results for covering a range of frequencies. Fractional derivatives can be introduced (see Wollscheid and Lion (2014) and reference therein) and Payne effect can also be represented (see for instance Lion and Kardelky (2004)). To the authors opinion, a disadvantage of this approach is that the link with the fundamental thermodynamical principles is not straightforward and can eventually lead to non admissible models. The last two approaches share the same concept using the introduction of internal variables to describe inelastic effects. Behind these variables, the local (in time and in space) state hypothesis is used (see for instance Germain et al. (1983)) in the framework of the thermodynamics of irreversible processes. Approaches can be distinguished in the way that evolution equations are obtained. One can find micromechanically motivated models (see Reese (2003); Linder et al. (2011)), homogenization based model (see for instance Miehe and Göktepe (2005); Omnès et al. (2008)) and purely phenomenological models (see Rendek and Lion (2010) for Payne effect modeling within phenomenological models or Martinez et al. (2011) for a statistical representation of viscosity). In these approaches the link with fundamental thermodynamical principles is straightforward so as the numerical implementation in a finite element software.

The present model belongs to the last mentioned category. It constitutes an extension of a previously published model (see Delattre et al. (2014)). The starting point is to consider the rubber stress response as a sum of a nearly equilibrium response (which corresponds to the relaxed stress) and a finite number of non equilibrium ones (which correspond to a discrete spectrum of viscous stress, each one is associated to a characteristic time of viscosity). The equilibrium response is assumed to follow a classical nearly incompressible visco-plastic behavior and the non equilibrium ones are represented with an original isochoric viscous model that takes into account the dynamical softening due to Payne effect. The key points of the proposed approach are the introduction of tensorial viscosities and of damage like variables that represent the Payne effect. The tensorial viscous flow allows to take into account an effect of orientation of each viscous stresses relative to the global deformation. The characteristic times of viscosity are therefore not identical if one considers tension or shear. This approach allows a better phenomenological representation of multi-axial response and of mean stress (or preload) effect for cyclic harmonic tests (for these tests, the effect of the mean stress can be different in tension or shear). For Payne effect, it is considered isotropic internal variables which behave like damage variables. The Payne effect is commonly attributed to breakage of physically bonded filler network structure. The idea of a continuous breakage/reformation of the filler network during dynamical loading is at the origin of the so called Kraus model (Kraus et al. (1966)). The present evolution equations for damage like variables take into account characteristic times for Payne effect (dynamical softening can be found experimentally to not being instantaneous which is in contradiction with earlier approach of Kraus and co-workers) and is related to the maximal elastic strain energy seen during loading. A specific identification strategy is proposed to provide robust results with a relative

cheap numerical cost. A temperature dependency of the mechanical material parameters is deduced from identification results. The present model exhibits very promising results at various temperatures, various frequencies and amplitudes of loading both in tension/compression and in simple shear.

2. Experimental characterization

2.1. DMA and DSC results

The studied material is a butatiene rubber filled with carbon black, however the precise chemical composition and the processing conditions are not given due to industrial confidentiality. The filler ratio in mass is near 45% of the total mass (determined with thermogravimetric analysis). Figures 1 show Differential Scanning Calorimetry and Dynamical Mechanical Analysis results. The material homogeneity of the curing process has been checked in diabolo specimen by doing DSC analysis with two parts that were extracted from two different zones inside a diabolo: in the center and near an edge. It can be seen from figure 1(a) that the material is homogeneous inside the sample (the gap between both curves can be attributed to a difference of initial referential). It can be seen that the glass-transition temperature is located near -85^oC

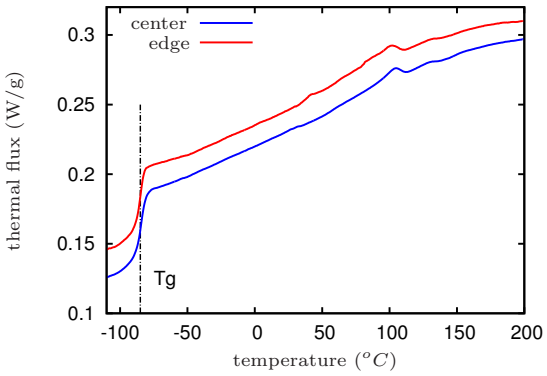

(a) Differential Scanning Calorimetry. DSC has been performed on samples that are extracted from different locations of a diabolo specimen: in the center and on an edge.

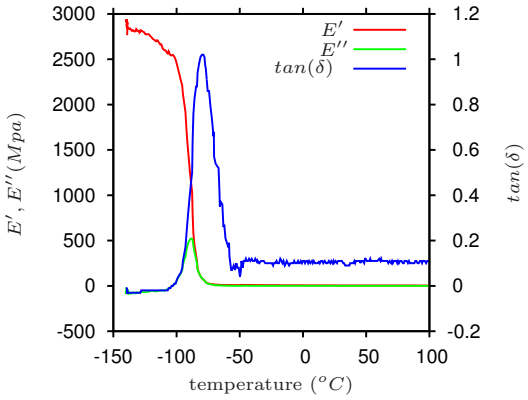

(b) Dynamical Mechanical Analysis: temperature scanning

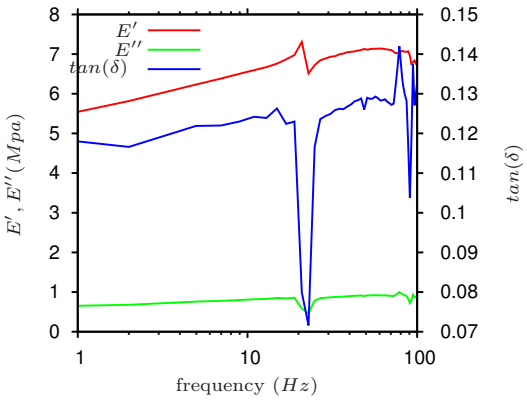

(c) Dynamical Mechanical Analysis: frequency scanning (T=25^oC). The discontinuity of the modulus and of $tan(\delta)$ near $25Hz$ is artificial and due to the experimental setup.

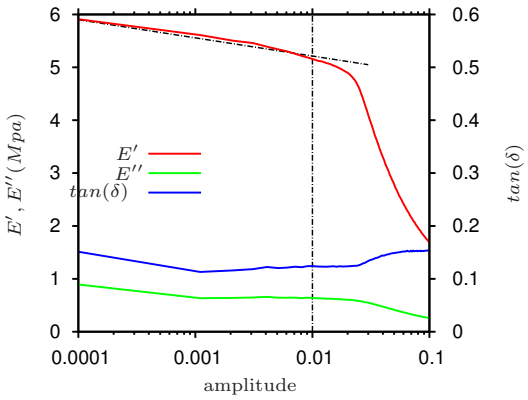

(d) Dynamical Mechanical Analysis: amplitude scanning (T=25^oC)

Figure 1: DSC and DMA analysis of the studied material.

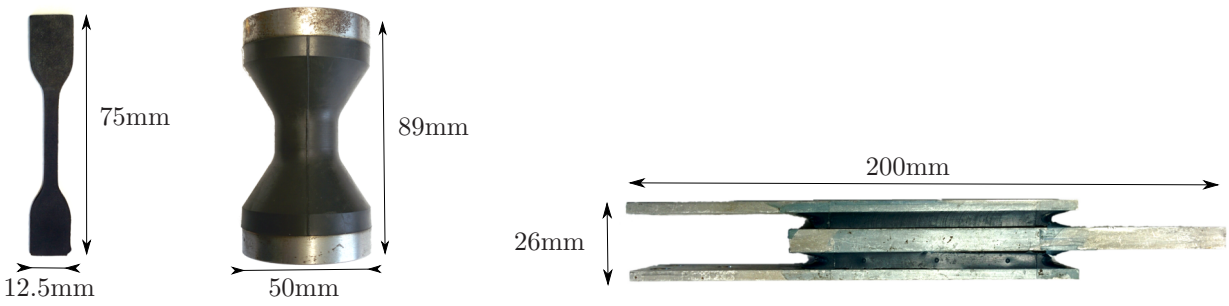

Figure 2: Specimens, left from right: H2, diabolo and double-shear.

and that the frequency dependency is almost linear (in the range 1 to 100Hz) in the linear regime of the material (*i.e.* for an amplitude smaller than 1%).

2.2. Experimental setup in the non-linear regime

In the non-linear regime (for larger strain), the behavior is characterized from cyclic and monotonic (relaxation) tests that have been done on double-shear, diabolo and tension (H2) specimens. These tests have been done with electro-mechanic or hydraulic testing machines equipped with temperature controlled adiabatic chambers. Figure 2 shows the geometry and the characteristic dimensions of each specimen.

The temperature of the samples is obviously not controlled and can evolve due to thermo-mechanical couplings (the temperature of the sample is not recorded). For cyclic tests, we consider that the self-heating phenomenon does not have sufficient time to develop significantly. For all tests, the samples are "De-Mullinized" by doing 20 cycles at a small strain rate and at a larger amplitude than the maximum amplitude seen by the material during characterization. Subsequent to this, a relaxation period is observed (30 min) to remove viscous effects before characterization tests. To check the experimental repeatability, each test has been run on two different specimens.

2.3. Equilibrium hysteresis

Figures 3 show the equilibrium hysteresis in shear or tension at different temperatures. The equilibrium hysteresis (see for instance Lion (1996)) are obtained by interrupting a constant strain rate load and unload test with relaxation periods of 90 minutes. The equilibrium stresses obtained at the end of each relaxation period form an hysteresis loop. For this test, as a long relaxation period is observed it can be safely assumed that the temperature of the material at equilibrium (at the end of each relaxation) is strictly equal to the ambient temperature. If this hysteresis area is null or quasi null the behavior can be said to be perfectly viscoelastic (or perfectly thermo-elastic). A contrario, if the hysteresis area can't be neglected the material exhibits more complex dissipative phenomena (crystallization, damage, ...). For the studied material, the equilibrium hysteresis area is very small for positive temperatures and the behavior is assumed to be mainly viscoelastic. For a negative temperature the hysteresis area can't be neglected. Considering the influence of the temperature on the value of equilibrium stresses it can be remarked that both for tension and shear the stress increases upon temperature. This effect is characteristic of the entropic elasticity nature of the rubber materials.

2.4. Dynamic stabilized response and Payne effect

Typical stabilized responses for harmonic loadings in shear and tension are shown in the figures 4. These tests are run for a frequency range from 3Hz to 25Hz and an amplitude range from 0.1 to 1.0 which correspond to the operating conditions seen by rubber parts in helicopter rotors. Furthermore the influence of the mean stress is studied by applying a non-null mean strain.

To analyze the results it is proposed to focus on the evolution of the hysteresis area (in MPa) and of a dynamic modulus (in MPa) which is defined in shear by the slope of the secant line of the hysteresis and in

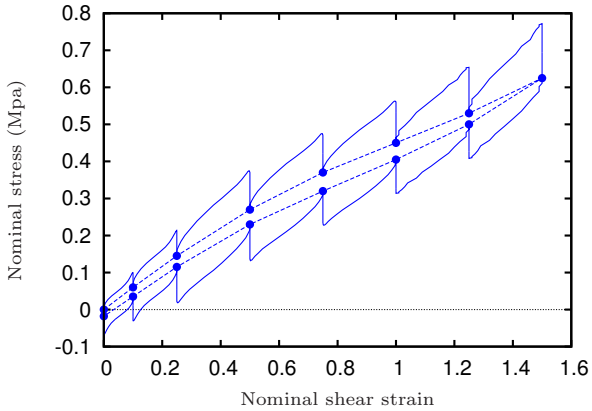

(a) Simple shear result at 20^oC (on double shear specimens)

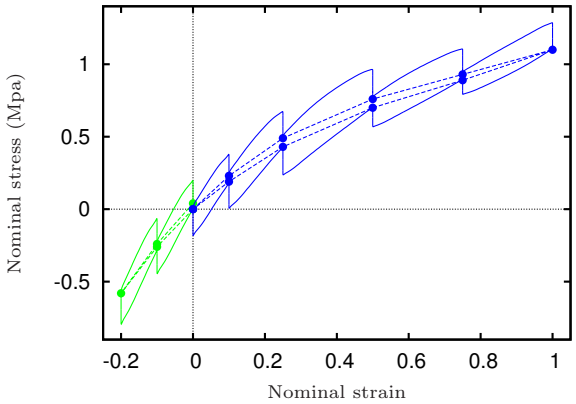

(b) Tension/Compression result at 20^oC (on diabolo specimens)

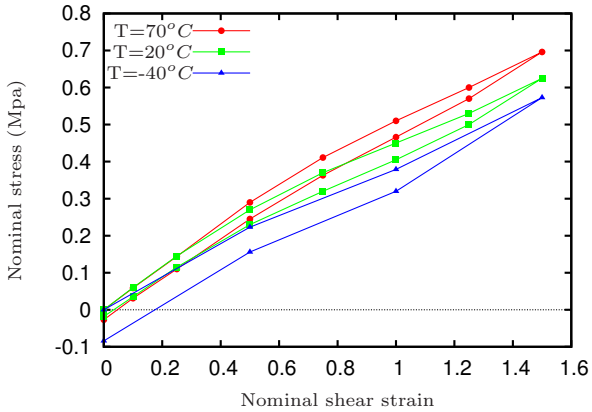

(c) Simple shear results for various temperatures: only relaxed stress are shown (on double shear specimens)

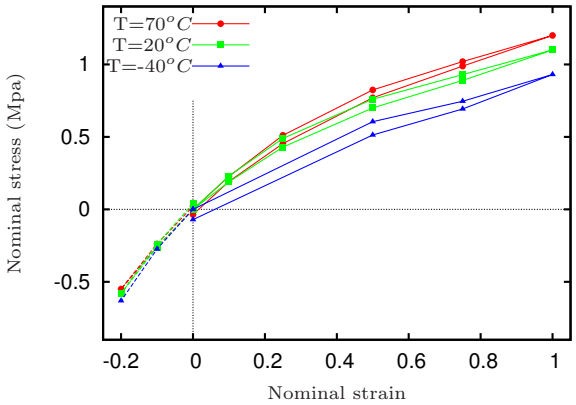

(d) Tension/Compression results for various temperatures: only relaxed stress are shown (on diabolo specimens)

Figure 3: Equilibrium hysteresis: each point is obtained by taking the equilibrium stress of a relaxation test

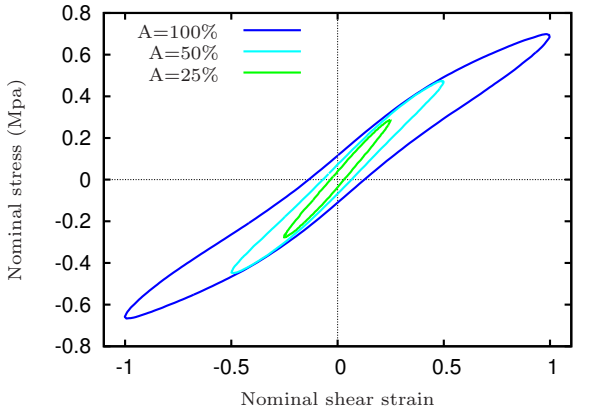

(a) Simple shear results (on double shear specimens)

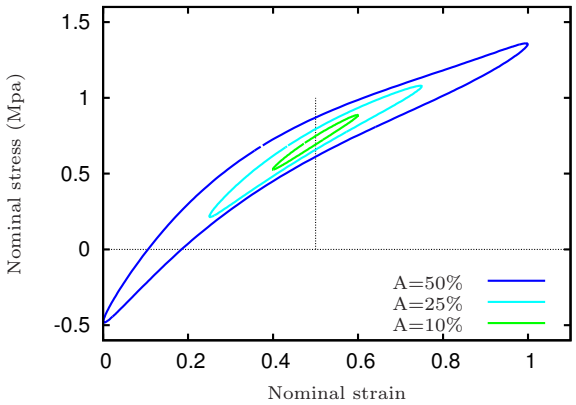

(b) Tension/Compression results (on diabolo specimens)

Figure 4: Stabilized hysteresis for a sinusoidal loading at various amplitudes for a frequency of $3Hz$ at 20^oC

tension by the slope of a line which starts from the mean strain point and ends in max strain point. The Payne effect is clearly observed from the curves: 5, for a given frequency the dynamic modulus decreases as the loading amplitude increases. This effect seems sensitive to the environmental temperature as it becomes stronger for negative temperatures (this is more sensitive in shear than in tension). It is well known that the Payne effect is at least partially recoverable: if one runs harmonic tests with progressive amplitudes followed by decreasing amplitudes it can be observed that the dynamic modulus respectively decreases and increases. Figures 6 show that the reversibility of the Payne effect is partial (not instantaneous) and does not seem sensitive to the frequency.

For a given frequency and a given amplitude it can be noticed a thermal softening effect (stress decreases as temperature increases), this effect is opposite to the entropic behavior observed for the equilibrium hysteresis.

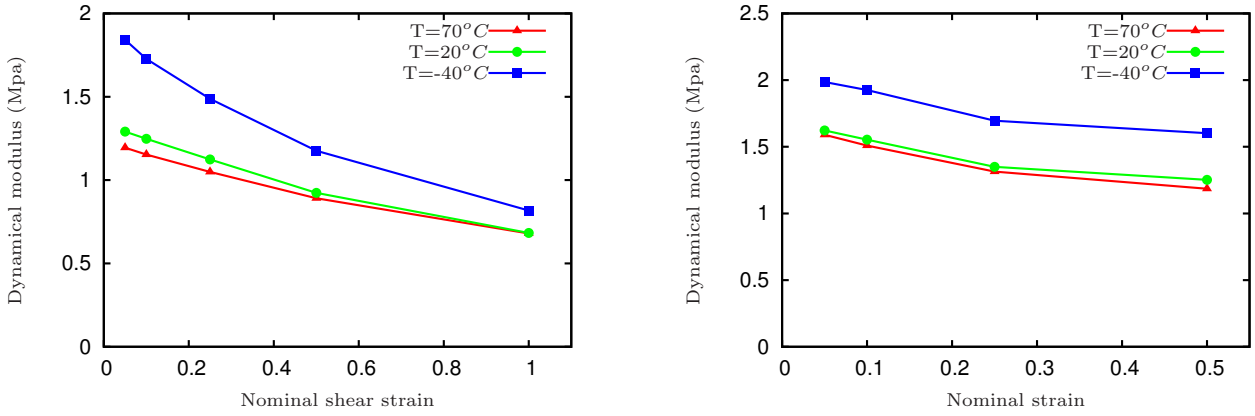

(a) Simple shear results (on double shear specimens)

(b) Tension/Compression results (on diabolo specimens)

Figure 5: Dynamic modulus at various amplitudes and various temperature for a frequency of $3Hz$: influence of the Payne effect

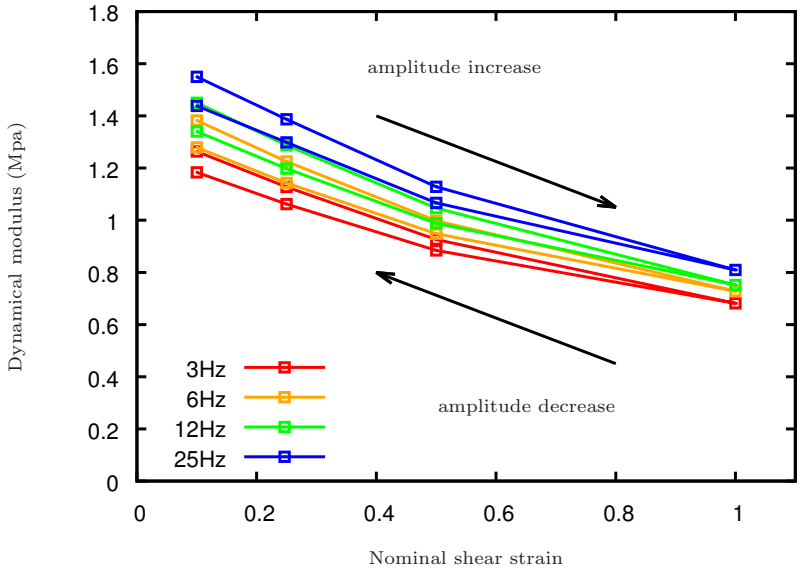

Figure 6: Reversibility of the Payne effect at $20°C$ in simple shear.

Figures 7 and 8 show that the material response is less sensitive to the frequency of loading (in the

range 3Hz to 25Hz) than of the amplitude of loading. Furthermore the thermal softening effect seems not dependent on the frequency.

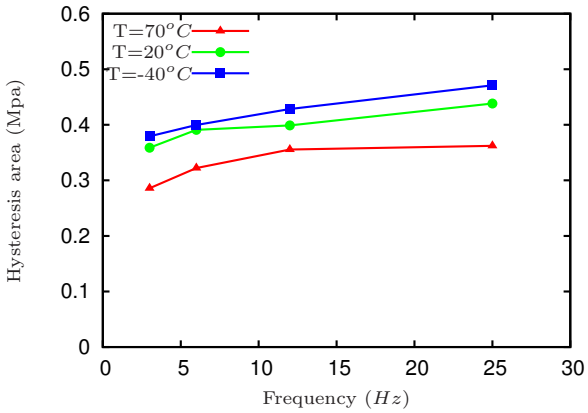

(a) Simple shear results (on double shear specimens)

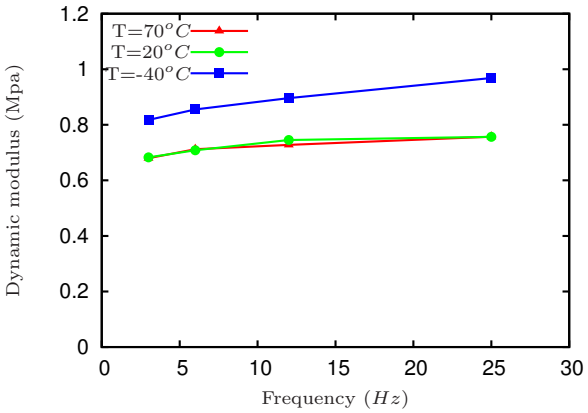

(b) Simple shear results (on double shear specimens)

Figure 7: Dynamic modulus and hysteresis area at various frequencies and various temperatures in simple shear ($\gamma = \pm 1$)

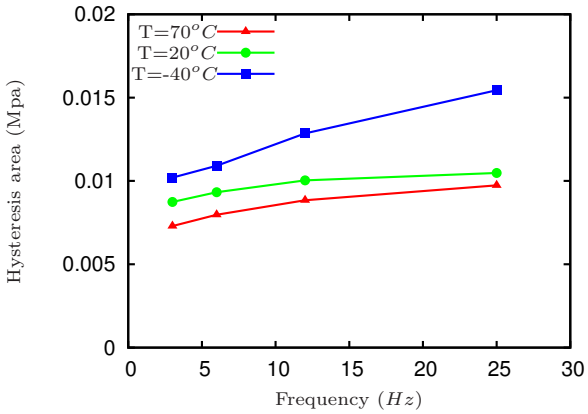

(a) Tension/Compression results (on diabolo specimens)

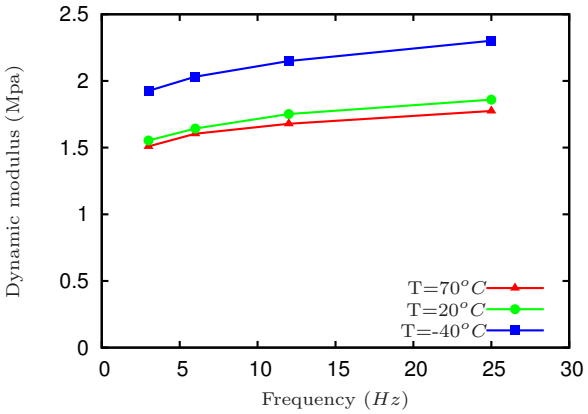

(b) Tension/Compression results (on diabolo specimens)

Figure 8: Dynamic modulus and hysteresis area at various frequencies and various temperatures in tension $\lambda_{max} = 1.6, \lambda_{min} = 1.4$ (diabolo specimen)

The effect of the mean strain is shown in the figures 9 and 10. It can be observed that tension specimens are more sensitive to this effect than double shear specimens. Increasing mean strain leads to a softening and to a decrease of the hysteresis area. This effect is non-linear and accentuated when harmonic amplitudes are small compared to the mean strain value.

3. Constitutive Modeling

3.1. Preliminary

The tensorial notations and operators used in the following are summed up in the table 1.

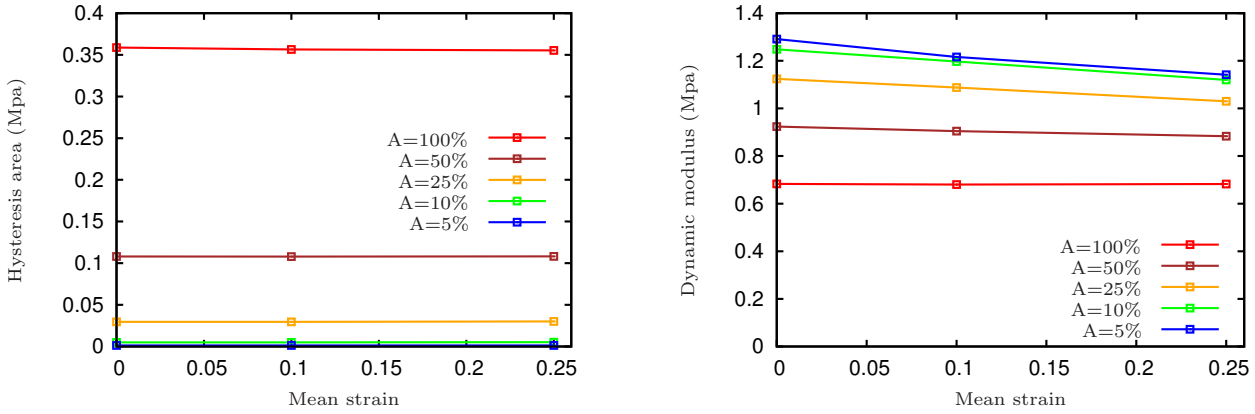

(a) Hysteresis area (b) Dynamic modulus

Figure 9: Effect of the mean strain on the dynamical response for various amplitudes at 3Hz and 20^oC in simple shear

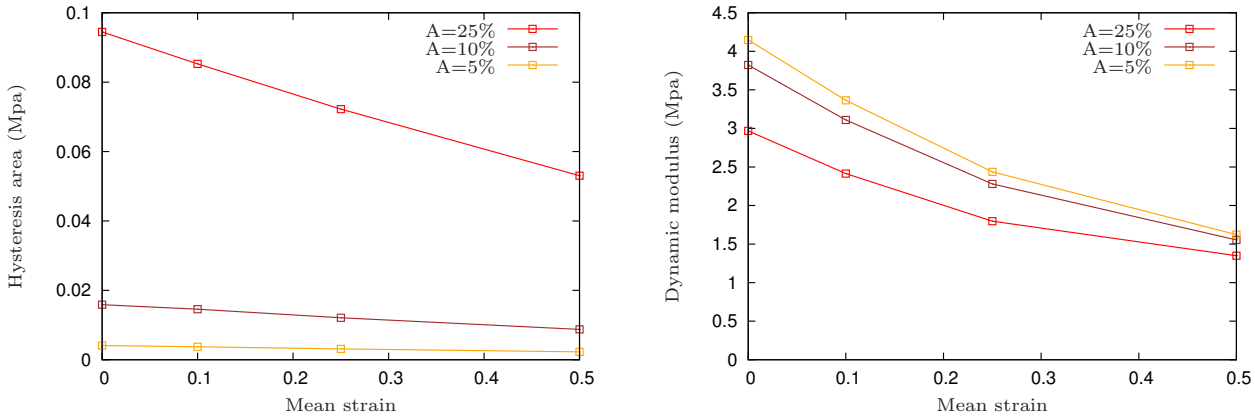

(a) Hysteresis area (b) Dynamic modulus

Figure 10: Effect of the mean strain on the dynamical response for various amplitudes at 3Hz and 20^oC in tension (diabolo specimen)

symbol	definition
$\cdot$	simple contraction: $\mathbf{A}\cdot\mathbf{B} = A_{ij}B_{jk}$
$:$	double contraction: $\mathbf{A}:\mathbf{B} = A_{ij}B_{ij}$
$^{\mathrm{T}}$	transpose operator: $\mathbf{A}^{\mathrm{T}} = A^{\mathrm{T}}_{ij} = A_{ji}$
tr	trace operator: $\mathrm{tr}\mathbf{A} = A_{ii}$
$^{\mathrm{D}}$	deviatoric operator: $\mathbf{A}^{\mathrm{D}} = A^{\mathrm{D}}_{ij} = A_{ij} - \frac{1}{3}A_{kk}\delta_{ij}$
$\|A\|$	a tensorial norm: $\|A\| = \sqrt{\mathbf{A}:\mathbf{A}}$
$\otimes$	tensorial product: $\mathbf{a}\otimes\mathbf{b} = a_i b_j$
$\odot$	defined by $(A\odot B)_{ijkl} = A_{ik}B_{jl}$

Table 1: Tensorial notations and symbols

3.2. Kinematic

The proposed constitutive model is based on the thermodynamics of irreversible processes and on the local state assumption: local both in time and in spatial position. Therefore to model irreversible effects it is introduced internal variables which depend on the current time t and the current position $\mathbf{x}(t)$. The initial

position of a material point is noted $\mathbf{X}$. The initial state is assumed to be an equilibrium free stress state. At all times there exists an unique and invertible mapping between the current and the initial position: $\mathbf{x} = \mathcal{X}(\mathbf{X}, t)$. The gradient of this mapping is called deformation gradient: $\mathbf{F} = \partial\mathcal{X}(\mathbf{X}, t)/\partial\mathbf{X}$. Following Flory (1961), the deformation gradient is splited into a volumetric and an isochoric part, the isochoric transformation is also multiplicatively decomposed into a purely elastic part and an inelastic one (in the present approach inelastic deformation can be viscosity, $\bar{\mathbf{F}}_\mathbf{v}$, or plasticity, $\bar{\mathbf{F}}_\mathbf{p}$):

$$\mathbf{F} = (J^{1/3})\bar{\mathbf{F}} = (J^{1/3})\bar{\mathbf{F}}_\mathbf{e} \cdot \bar{\mathbf{F}}_\mathbf{v} = (J^{1/3})\bar{\mathbf{F}}_\mathbf{ep} \cdot \bar{\mathbf{F}}_\mathbf{p} \tag{1}$$

Where $\bar{\mathbf{F}}_\mathbf{e}$, $\bar{\mathbf{F}}_\mathbf{ep}$ denote elastic isochoric deformation gradients associated to viscosity or plasticity respectively. It is implicitly assumed from the previous equation that no dissipative mechanisms occur for volumetric deformation. In the intend to reproduce the material behavior, we use a phenomenological approach in which n mechanisms of dissipation are combined together (multiple relaxation times or multiple behaviors). Therefore, eq (1) is generalized to the case of the n elastic and inelastic deformation gradients such that:

$$\mathbf{F} = (J^{1/3})\bar{\mathbf{F}}^i_\mathbf{e} \cdot \bar{\mathbf{F}}^i_\mathbf{v} \qquad i = 1..n \tag{2}$$

3.3. Thermodynamical framework

To proceed further, it is made the following hypotheses:

- Only isothermal conditions are considered: temperature is assumed to be homogeneous and fixed in time. Considering equilibrium hysteresis results this hypothesis seems correct as the material has sufficient time to diffuse thermal flux due to thermo-mechanical couplings. For cyclic test, it is clear that this hypothesis is strong as the temperature inside the material will evolve (due to thermo-mechanical couplings and due to irreversible phenomena), however we assume that these evolutions are small regarding the short duration of a dynamical test. Therefore, we consider that the temperature of the material is closed to the ambient temperature (inside the adiabatic chamber) and we neglect the thermal dilatation;

- Following Bergström and Boyce (2000) among others, the Cauchy stress $\boldsymbol{\sigma}$ is assumed to be a sum of two contributions: $\boldsymbol{\sigma} = \boldsymbol{\sigma}_{eq} + \boldsymbol{\sigma}_v$ where $\boldsymbol{\sigma}_{eq}$ is the equilibrium stress (*i.e.* the stress obtain after removing viscous effects) and $\boldsymbol{\sigma}_v$ is the supplementary stress due to viscosity. The equilibrium part is phenomenologically represented by an elasto-visco-plastic behavior to take into account of very long time viscous processes and of the low mobility of polymer chains for negative temperatures. The supplementary viscous stress is assumed as a sum of a finite range of viscous stress responses, each response is associated to a characteristic time of viscosity (leading to the so-called Maxwell-generalized phenomenological approach).

- Payne effect is assumed to be irreversible: the present model don't take into account of the recovery of the Payne effect experimentally observed[1] (see figure 6). The Payne effect is also assumed as isotropic and n scalar internal variables are introduced (one per characteristic viscous time).

The Helmoltz free specific energy is chosen as follows:

$$\psi(\bar{\mathbf{B}}, \bar{\mathbf{B}}^i_\mathbf{e}, \bar{\mathbf{B}}_\mathbf{ep}, \omega_i, J, \Theta) = \psi_{eq}(\bar{\mathbf{B}}, \bar{\mathbf{B}}_\mathbf{ep}, \Theta) + \psi_{vis}(\bar{\mathbf{B}}^i_\mathbf{e}, \omega_i, \Theta) + \psi_{vol}(J) \qquad i = 1..n \tag{3}$$

where $\bar{\mathbf{B}} = \bar{\mathbf{F}} \cdot \bar{\mathbf{F}}^\mathrm{T}$, $\bar{\mathbf{B}}_\mathbf{ep} = \bar{\mathbf{F}}_\mathbf{ep} \cdot \bar{\mathbf{F}}^\mathrm{T}_\mathbf{ep}$ and $\bar{\mathbf{B}}^i_\mathbf{e} = \bar{\mathbf{F}}^i_\mathbf{e} \cdot \bar{\mathbf{F}}^{i^\mathrm{T}}_\mathbf{e}$ are the elastic, elasto-plastic and visco-elastic left Cauchy Green tensors, Θ is the absolute temperature (in Kelvin). The scalar internal variables ω_i represent the Payne effect: they evolve from $\omega_i(t = 0) = 1$ to a positive value smaller than one depending on the applied amplitude. The energies ψ_{eq}, ψ_{vol}, ψ_{vis} and ψ_Θ are respectively the equilibrium, the volumic, the viscous and the thermal (heat storage term) free specific energies.

[1] To the authors knowledge, there is a lack in the literature concerning modelization of the partial recovery of Payne effect

Neglecting thermal dissipation (conductivity or heat flow) and temperature evolution, the combination of the first and the second laws of thermodynamics leads to the following inequality (Clausius-Duhem form):

$$\phi = \boldsymbol{\sigma} : \mathbf{D} - \rho\dot{\psi} \geq 0 \quad \forall \mathbf{D} \tag{4}$$

where $\mathbf{D}$ is the eulerian strain rate: $\mathbf{D} = 1/2(\mathbf{L} + \mathbf{L}^{\mathrm{T}})$ with $\mathbf{L} = \dot{\mathbf{F}} \cdot \mathbf{F}^{-1}$ and ρ is the current density. The dot symbol in eq. (4) or in the previous definition of the strain rate stands for the so-called material time derivative: derivative of quantity upon time holding initial position constant. The material time derivative of the free energy defined in eq. (3) is:

$$\dot{\psi} = \frac{\partial \psi_{eq}}{\partial \bar{\mathbf{B}}} : \dot{\bar{\mathbf{B}}} + \frac{\partial \psi_{eq}}{\partial \bar{\mathbf{B}}_{\mathbf{ep}}} : \dot{\bar{\mathbf{B}}}_{\mathbf{ep}} + \sum_{i=1}^{n} \frac{\partial \psi_{vis}}{\partial \bar{\mathbf{B}}^i_{\mathbf{e}}} : \dot{\bar{\mathbf{B}}}_{\mathbf{e}}^{\ i} + \sum_{i=1}^{n} \frac{\partial \psi_{vis}}{\partial \omega^i}\dot{\omega}^i + \frac{\partial \psi_{vol}}{\partial J}\dot{J} \tag{5}$$

Using the definition of Cauchy tensor and the relations (1) and (2), one can obtain the following relations:

$$\dot{\bar{\mathbf{B}}} = \mathbf{L} \cdot \bar{\mathbf{B}} + \bar{\mathbf{B}} \cdot \mathbf{L}^{\mathrm{T}} - \frac{2}{3}(\mathbf{1} : \mathbf{D})\bar{\mathbf{B}} \tag{6}$$

$$\dot{\bar{\mathbf{B}}}_{\mathbf{e}}^{\ i} = \mathbf{L} \cdot \bar{\mathbf{B}}^i_{\mathbf{e}} + \bar{\mathbf{B}}^i_{\mathbf{e}} \cdot \mathbf{L}^{\mathrm{T}} - 2\bar{\mathbf{V}}^i_{\mathbf{e}} \cdot \bar{\mathbf{D}}^{\mathbf{o}^i}_{\mathbf{v}} \cdot \bar{\mathbf{V}}^i_{\mathbf{e}} - \frac{2}{3}(\mathbf{1} : \mathbf{D})\bar{\mathbf{B}}^i_{\mathbf{e}}, \quad i = 1..n \tag{7}$$

$$\dot{\bar{\mathbf{B}}}_{\mathbf{ep}} = \mathbf{L} \cdot \bar{\mathbf{B}}_{\mathbf{ep}} + \bar{\mathbf{B}}_{\mathbf{ep}} \cdot \mathbf{L}^{\mathrm{T}} - 2\bar{\mathbf{V}}_{\mathbf{ep}} \cdot \bar{\mathbf{D}}^{\mathbf{o}}_{\mathbf{p}} \cdot \bar{\mathbf{V}}_{\mathbf{ep}} - \frac{2}{3}(\mathbf{1} : \mathbf{D})\bar{\mathbf{B}}_{\mathbf{ep}} \tag{8}$$

where $\mathbf{1}$ is the second order unit tensor and $\bar{\mathbf{V}}^i_{\mathbf{e}}$, $\bar{\mathbf{V}}_{\mathbf{ep}}$ come from the polar decompositions: $\bar{\mathbf{F}}^i_{\mathbf{e}} = \bar{\mathbf{V}}^i_{\mathbf{e}} \cdot \bar{\mathbf{R}}^i_{\mathbf{e}}$ and $\bar{\mathbf{F}}_{\mathbf{ep}} = \bar{\mathbf{V}}_{\mathbf{ep}} \cdot \bar{\mathbf{R}}_{\mathbf{ep}}$.
The material time derivative of the volume variation is given by:

$$\dot{J} = J(\mathbf{1} : \mathbf{D}) \tag{9}$$

In eq. (7) and (8), objective eulerian strain rates have been introduced. These rate are defined from:

$$\bar{\mathbf{D}}^{\mathbf{o}^i}_{\mathbf{v}} = \bar{\mathbf{R}}^i_{\mathbf{e}} \cdot \bar{\mathbf{D}}^i_{\mathbf{v}} \cdot \bar{\mathbf{R}}^{i^{\mathrm{T}}}_{\mathbf{e}} \qquad \bar{\mathbf{D}}^{\mathbf{o}}_{\mathbf{p}} = \bar{\mathbf{R}}_{\mathbf{ep}} \cdot \bar{\mathbf{D}}_{\mathbf{p}} \cdot \bar{\mathbf{R}}^{\mathrm{T}}_{\mathbf{ep}} \tag{10}$$

Inserting (5) to (9) in (4) and after using some symmetry properties and reordering terms, the Clausius-Duhem inequality is written as:

$$\begin{aligned} \phi = & \overbrace{\left(\boldsymbol{\sigma} - 2\rho\left(\bar{\mathbf{B}} \cdot \frac{\partial \psi_{eq}}{\partial \bar{\mathbf{B}}} + \bar{\mathbf{B}}_{\mathbf{ep}} \cdot \frac{\partial \psi_{eq}}{\partial \bar{\mathbf{B}}_{\mathbf{ep}}} + \sum_{i=1}^{n} \bar{\mathbf{B}}^i_{\mathbf{e}} \cdot \frac{\partial \psi_{vis}}{\partial \bar{\mathbf{B}}^i_{\mathbf{e}}}\right)^{\mathrm{D}} - \rho J \frac{\partial \psi_{vol}}{\partial J}\mathbf{1}\right) : \mathbf{D}}^{\phi_0} \\ & \underbrace{+ 2\rho \sum_{i=1}^{n}\left(\bar{\mathbf{B}}^i_{\mathbf{e}} \cdot \frac{\partial \psi_{vis}}{\partial \bar{\mathbf{B}}^i_{\mathbf{e}}}\right) : \bar{\mathbf{D}}^{\mathbf{o}^i}_{\mathbf{v}}}_{\phi_{vis}} + \underbrace{2\rho\left(\bar{\mathbf{B}}_{\mathbf{ep}} \cdot \frac{\partial \psi_{eq}}{\partial \bar{\mathbf{B}}_{\mathbf{ep}}}\right) : \bar{\mathbf{D}}^{\mathbf{o}}_{\mathbf{p}}}_{\phi_{eq}} + \underbrace{\sum_{i=1}^{n} -\rho \frac{\partial \psi_{vis}}{\partial \omega^i}\dot{\omega}^i}_{\phi_{payne}} \geq 0 \\ & \qquad\qquad\qquad\qquad\qquad\qquad\qquad\qquad\qquad\qquad\qquad\qquad \forall \mathbf{D}, \bar{\mathbf{D}}^{\mathbf{o}^i}_{\mathbf{v}}, \bar{\mathbf{D}}^{\mathbf{o}}_{\mathbf{p}}, \dot{\omega}^i \end{aligned} \tag{11}$$

As each thermodynamical flow is independent from each other in the previous expression, we consider that the positivity of each dissipation term is independently required: $\phi_0 \geq 0$, $\phi_{eq} \geq 0$, $\phi_{vis} \geq 0$, $\phi_{payne} \geq 0$. Furthermore, as it is assumed that mechanical irreversibilities are fully represented by internal variables, it

is stated that $\phi_0 = 0$. Therefore, the Clausius-Duhem inequality is satisfied if:

$$\boldsymbol{\sigma} = \overbrace{2\rho\left(\bar{\mathbf{B}}\cdot\frac{\partial\psi_{eq}}{\partial\bar{\mathbf{B}}}+\bar{\mathbf{B}}_{\mathbf{ep}}\cdot\frac{\partial\psi_{eq}}{\partial\bar{\mathbf{B}}_{\mathbf{ep}}}\right)^{\mathrm{D}}+\rho J\frac{\partial\psi_{vol}}{\partial J}\mathbf{1}}^{\boldsymbol{\sigma}_{eq}}+\sum_{i=1}^{n}\overbrace{2\rho\left(\bar{\mathbf{B}}^i_{\mathbf{e}}\cdot\frac{\partial\psi_{vis}}{\partial\bar{\mathbf{B}}^i_{\mathbf{e}}}\right)^{\mathrm{D}}}^{\boldsymbol{\sigma}^i_v} \tag{12}$$

$$\phi_{eq} = 2\rho\left(\bar{\mathbf{B}}_{\mathbf{ep}}\cdot\frac{\partial\psi_{eq}}{\partial\bar{\mathbf{B}}_{\mathbf{ep}}}\right):\bar{\mathbf{D}}^{\mathbf{o}}_{\mathbf{p}}\geq 0 \tag{13}$$

$$\phi^i_{vis} = 2\rho\left(\bar{\mathbf{B}}^i_{\mathbf{e}}\cdot\frac{\partial\psi_{vis}}{\partial\bar{\mathbf{B}}^i_{\mathbf{e}}}\right):\bar{\mathbf{D}}^{\mathbf{o}^i}_{\mathbf{v}}\geq 0 \qquad i=1..n \tag{14}$$

$$\phi^i_{payne} = -\rho\frac{\partial\psi_{vis}}{\partial\omega^i}\dot{\omega}^i\geq 0 \qquad i=1..n \tag{15}$$

$$\tag{16}$$

3.4. Equilibrium contribution

It is considered the elastic domain: $\mathbb{E} = \{\boldsymbol{\sigma}_p | f(\boldsymbol{\sigma}_p,\Theta)\leq 0\}$ defined by the following yield function:

$$f(\boldsymbol{\sigma}_p,\Theta) = \|\boldsymbol{\sigma}_p\| - \chi(\Theta) \qquad \text{with} \qquad \boldsymbol{\sigma}_p = 2\rho\left(\bar{\mathbf{B}}_{\mathbf{ep}}\cdot\frac{\partial\psi_{eq}}{\partial\bar{\mathbf{B}}_{\mathbf{ep}}}\right)^{\mathrm{D}} \tag{17}$$

where χ is the yield parameter that depends on temperature. The plastic flow rule is defined from:

$$\bar{\mathbf{D}}^{\mathbf{o}}_{\mathbf{p}} = \frac{<f(\boldsymbol{\sigma}_p,\Theta)>}{\zeta(\Theta)}\frac{\boldsymbol{\sigma}_p}{\|\boldsymbol{\sigma}_p\|} \tag{18}$$

where $<.>$ denotes the Macaulay brackets[2] and $\zeta(\Theta)$ is a viscosity like parameter ($\zeta(\Theta)\geq 0$). The proof of the thermodynamical admissibility of (18) is straight forward: inserting (18) in (13) leads to:

$$\phi_{eq} = \frac{<f(\boldsymbol{\sigma}_p,\Theta)>}{\zeta(\Theta)}\frac{\boldsymbol{\sigma}_p:\boldsymbol{\sigma}_p}{\|\boldsymbol{\sigma}_p\|}\geq 0 \tag{19}$$

The equilibrium and volumic free energies are chosen as follows:

$$\begin{aligned}\rho_0\psi_{eq} &= C_1(\Theta)\left(I_1(\bar{\mathbf{B}})-3\right)+C_2(\Theta)\left(I_2(\bar{\mathbf{B}})-3\right)+G_p(\Theta)(I_1(\bar{\mathbf{B}}_{\mathbf{ep}})-3)\\ \rho_0\psi_{vol} &= \frac{k}{2}(\ln J)^2\end{aligned} \tag{20}$$

The material parameters C_1, C_2, G_p are assumed to be dependent on temperature. Due to the lack of experimental data the bulk modulus k is assumed to be independent on the temperature. The strain invariants are defined from $I_1(\mathbf{X}) = \mathrm{Tr}(\mathbf{X})$ and $I_2(\mathbf{X}) = 1/2((\mathrm{Tr}(\mathbf{X}))^2 - \mathrm{Tr}(\mathbf{X}\cdot\mathbf{X})$. The initial density ρ_0 is related to the current one from: $\rho = J^{-1}\rho_0$. Using the previous definition, the equilibrium stress is written as:

$$\boxed{\boldsymbol{\sigma}_{eq} = J^{-1}\left(2C_1(\Theta)\bar{\mathbf{B}}^{\mathrm{D}}+2C_2(\Theta)(I_1(\bar{\mathbf{B}})\bar{\mathbf{B}}-\bar{\mathbf{B}}^2)^{\mathrm{D}}+2G_p(\Theta)\bar{\mathbf{B}}^{\mathrm{D}}_{\mathbf{ep}}+k\ln J\mathbf{1}\right)} \tag{21}$$

Inserting (18) in (8) it is obtained the following flow rule:

$$\boxed{\dot{\bar{\mathbf{B}}}_{\mathbf{ep}} = \mathbf{L}\cdot\bar{\mathbf{B}}_{\mathbf{ep}}+\bar{\mathbf{B}}_{\mathbf{ep}}\cdot\mathbf{L}^{\mathrm{T}}-\frac{2}{3}(\mathbf{1}:\mathbf{L})\bar{\mathbf{B}}_{\mathbf{ep}}-2\frac{<f(\boldsymbol{\sigma}_p,\Theta)>}{\zeta(\Theta)}\frac{\bar{\mathbf{B}}_{\mathbf{ep}}\cdot\bar{\mathbf{B}}^{\mathrm{D}}_{\mathbf{ep}}}{\|\bar{\mathbf{B}}^{\mathrm{D}}_{\mathbf{ep}}\|}} \tag{22}$$

[2]Macaulay brackets are defined from: $<f>=f$ if $f\geq 0$ and $<f>=0$ elsewhere.

3.5. Time dependent contribution (non isotropic viscous flows)

In the present contribution it is proposed an original approach to take into account of the influence of loading directions on the viscous flow. The original idea that has been developed in a previous paper (see Delattre et al. (2014)) is to consider that viscous mechanisms may be different in tension and in shear. One can imagine that an amorphous polymers like synthetic rubbers will become more and more structured (oriented chains) submitted to monotonic loading in tension. In shear this internal reorganization should be different. Therefore we have proposed a tensorial viscosity flow rule that distinguishes tension from shear. In this paper we adopt a more general approach by considering two mechanisms of viscosity: the first one is isotropic and the second one is dependent on the global strain direction through the eigenvectors of $\bar{\mathbf{B}}^{\mathrm{D}}$. When strain principal directions are aligned with viscous stress principal directions a classical Maxwell flow rule is obtained (in tension for instance). For other cases of loading the proposed form leads to a non classical viscosity (in shear for instance) for which the relaxation times may not be the same in each material direction. It is defined first the spectral representation of $\bar{\mathbf{B}}^{\mathrm{D}}$:

$$\bar{\mathbf{B}}^{\mathrm{D}} = \sum_{a=1}^{3} \lambda_a \mathbf{n_a} \otimes \mathbf{n_a} \tag{23}$$

The i^{th} viscous stress is defined by:

$$\boldsymbol{\sigma}_v^i = 2\rho \left(\bar{\mathbf{B}}_{\mathbf{e}}^i \cdot \frac{\partial \psi_{vis}}{\partial \bar{\mathbf{B}}_{\mathbf{e}}^i} \right)^{\mathrm{D}} \tag{24}$$

Introducing the temperature dependent parameters $\eta_1^i(\Theta, \omega_i)$ and $\eta_2^i(\Theta, \omega_i)$ it is proposed the following non-classical viscous flow rule:

$$\bar{\mathbf{D}}_{\mathbf{v}}^{\mathbf{o}^i} = \overbrace{\left(\frac{1}{\eta_1^i(\Theta,\omega_i)} \mathbb{I} + \left(\frac{1}{\eta_2^i(\Theta,\omega_i)} - \frac{1}{\eta_1^i(\Theta,\omega_i)} \right) \sum_{a=1}^{3} \mathbf{n_a} \otimes \mathbf{n_a} \otimes \mathbf{n_a} \otimes \mathbf{n_a} \right)}^{\mathbb{H}} : \boldsymbol{\sigma}_v^i \quad i = 1..n \tag{25}$$

where $\mathbb{I}$ is the fourth order identity tensor and $\eta_1^i(\Theta, \omega_i) \geq \eta_2^i(\Theta, \omega_i) \, \forall \Theta, \omega_i$.
The positivity of the dissipation can be shown by introducing (25) in (14):

$$\phi_{vis}^i = \boldsymbol{\sigma}_v^i : \mathbb{H} : \boldsymbol{\sigma}_v^i = \frac{1}{\eta_1^i(\Theta,\omega_i)} (\boldsymbol{\sigma}_v^i : \boldsymbol{\sigma}_v^i) + \left(\frac{1}{\eta_2^i(\Theta,\omega_i)} - \frac{1}{\eta_1^i(\Theta,\omega_i)} \right) \left(\mathbf{n_a} \cdot \boldsymbol{\sigma}_v^i \cdot \mathbf{n_a} \right) : \left(\mathbf{n_a} \cdot \boldsymbol{\sigma}_v^i \cdot \mathbf{n_a} \right) \geq 0 \tag{26}$$

Obviously we have considered that η_1^i and η_2^i are positives (and $\eta_1^i \geq \eta_2^i$). The material objectivity of the relation (25) can be shown by considering a transformation $\mathbf{F}^* = \mathbf{Q} \cdot \mathbf{F}$, $\bar{\mathbf{F}}_{\mathbf{e}}^{i^*} = \mathbf{Q} \cdot \bar{\mathbf{F}}_{\mathbf{e}}^i \cdot \mathbf{Q_1}$, $\bar{\mathbf{F}}_{\mathbf{v}}^i = {\mathbf{Q_1}}^{\mathrm{T}} \cdot \bar{\mathbf{F}}_{\mathbf{v}}^i$ where $\mathbf{Q}, \mathbf{Q_1}$ are orthogonal rotation tensors. Therefore, the direction vectors ${\mathbf{n_a}}^*$ are defined by ${\mathbf{n_a}}^* = \mathbf{Q} \cdot \mathbf{n_a}$ and it is obtained[3]:

$$\begin{aligned}
\bar{\mathbf{D}}_{\mathbf{v}}^{\mathbf{o}^{i^*}} &= \left(\frac{1}{\eta_1^i(\Theta,\omega_i)} \mathbb{I} + \left(\frac{1}{\eta_2^i(\Theta,\omega_i)} - \frac{1}{\eta_1^i(\Theta,\omega_i)} \right) \sum_{a=1}^{3} ({\mathbf{n_a}}^*) \otimes ({\mathbf{n_a}}^*) \otimes ({\mathbf{n_a}}^*) \otimes ({\mathbf{n_a}}^*) \right) : (\boldsymbol{\sigma}_v^{i^*}) \\
&= \left(\frac{1}{\eta_1^i(\Theta,\omega_i)} \mathbb{I} + \left(\frac{1}{\eta_2^i(\Theta,\omega_i)} - \frac{1}{\eta_1^i(\Theta,\omega_i)} \right) \sum_{a=1}^{3} (\mathbf{Q} \cdot \mathbf{n_a}) \otimes (\mathbf{Q} \cdot \mathbf{n_a}) \otimes (\mathbf{Q} \cdot \mathbf{n_a}) \otimes (\mathbf{Q} \cdot \mathbf{n_a}) \right) : (\mathbf{Q} \cdot \boldsymbol{\sigma}_v^i \cdot \mathbf{Q}^{\mathrm{T}}) \\
&= \left(\frac{1}{\eta_1^i(\Theta,\omega_i)} \mathbf{Q} \odot \mathbf{Q} + \left(\frac{1}{\eta_2^i(\Theta,\omega_i)} - \frac{1}{\eta_1^i(\Theta,\omega_i)} \right) \sum_{a=1}^{3} (\mathbf{Q} \cdot \mathbf{n_a}) \otimes (\mathbf{Q} \cdot \mathbf{n_a}) \otimes \mathbf{n_a} \otimes \mathbf{n_a} \right) : \boldsymbol{\sigma}_v^i \\
&= (\mathbf{Q} \odot \mathbf{Q}) : \left(\frac{1}{\eta_1^i(\Theta,\omega_i)} \mathbb{I} + \left(\frac{1}{\eta_2^i(\Theta,\omega_i)} - \frac{1}{\eta_1^i(\Theta,\omega_i)} \right) \sum_{a=1}^{3} \mathbf{n_a} \otimes \mathbf{n_a} \otimes \mathbf{n_a} \otimes \mathbf{n_a} \right) : \boldsymbol{\sigma}_v^i \\
&= (\mathbf{Q} \odot \mathbf{Q}) : \bar{\mathbf{D}}_{\mathbf{v}}^{\mathbf{o}^i} = \mathbf{Q} \cdot \bar{\mathbf{D}}_{\mathbf{v}}^{\mathbf{o}^i} \mathbf{Q}^{\mathrm{T}}
\end{aligned} \tag{27}$$

[3]One easily show that $\boldsymbol{\sigma}_v^{i^*} = \mathbf{Q} \cdot \boldsymbol{\sigma}_v^i \cdot \mathbf{Q}^{\mathrm{T}}$ as $\bar{\mathbf{B}}_{\mathbf{e}}^{i^*} = \bar{\mathbf{F}}_{\mathbf{e}}^{i^*} \cdot \bar{\mathbf{F}}_{\mathbf{e}}^{i^{\mathrm{T}*}} = \mathbf{Q} \cdot \bar{\mathbf{F}}_{\mathbf{e}}^i \cdot \mathbf{Q_1} \cdot {\mathbf{Q_1}}^{\mathrm{T}} \cdot \bar{\mathbf{F}}_{\mathbf{e}}^{i^{\mathrm{T}}} \cdot \mathbf{Q}^{\mathrm{T}} = \mathbf{Q} \cdot \bar{\mathbf{B}}_{\mathbf{e}}^i \cdot \mathbf{Q}^T$

which shows the demonstration of the objectivity of the chosen viscous flow. The isotropy can easily be shown as $\mathbf{n_a}$ are invariants by rotation of the referential.
The viscous free energy is chosen as:

$$\rho_0\psi_{vis} = \sum_{i=1}^{n} G_i(\Theta,\omega_i)(I_1(\bar{\mathbf{B}}^i_{\mathbf{e}}) - 3) \tag{28}$$

Therefore, the i^{th} viscous stress is written as:

$$\boxed{\boldsymbol{\sigma}^i_v = 2J^{-1}G_i(\Theta,\omega_i)\bar{\mathbf{B}}^{i\ \mathrm{D}}_{\mathbf{e}}} \qquad i = 1..n, \quad \omega_i \in]0,1] \tag{29}$$

Inserting (25) in (7) it is obtained:

$$\boxed{\begin{array}{l}\dot{\bar{\mathbf{B}}}^{\ i}_{\mathbf{e}} = \mathbf{L}\cdot\bar{\mathbf{B}}^i_{\mathbf{e}} + \bar{\mathbf{B}}^i_{\mathbf{e}}\cdot\mathbf{L}^{\mathrm{T}} - \dfrac{2}{3}(\mathbf{1}:\mathbf{L})\bar{\mathbf{B}}^i_{\mathbf{e}} - \dfrac{1}{J\tau^i_1}\bar{\mathbf{B}}^i_{\mathbf{e}}\cdot\bar{\mathbf{B}}^{i\ \mathrm{D}}_{\mathbf{e}} \\ \quad - \left(\dfrac{1}{J\tau^i_2} - \dfrac{1}{J\tau^i_1}\right)\displaystyle\sum_{a=1}^{3}(\bar{\mathbf{V}}^i_{\mathbf{e}}\cdot\mathbf{n_a})\otimes(\bar{\mathbf{V}}^i_{\mathbf{e}}\cdot\mathbf{n_a})(\mathbf{n_a}\cdot\bar{\mathbf{B}}^{i\ \mathrm{D}}_{\mathbf{e}}\cdot\mathbf{n_a}), \quad \bar{\mathbf{B}}^i_{\mathbf{e}}(t=0) = \mathbf{1}\end{array}} \quad i = 1..n \tag{30}$$

where $\tau^i_1 = \eta^i_1(\Theta,\omega_i)/4G_i(\Theta,\omega_i)$ and $\tau_2 = \eta_2(\Theta,\omega_i)/4G_i(\Theta,\omega_i)$ are the two characteristic times of viscosity linked to the i^{th} viscous stress. It is assumed that τ^i_1 and τ^i_2 do not depend on temperature (therefore shear modulus and viscosity have the same dependance in ω_i and Θ). Furthermore, as ω_i is a decreasing variable which takes one for initial value, it is chosen the following parametrization:

$$\boxed{G_i(\Theta,\omega_i) = \omega_i(g^l_i\Theta + g^c_i)} \quad i = 1..n \tag{31}$$

In the previous equation a linear temperature dependency of the neoHookean parameters is assumed (g^l_i and g^c_i are material parameters to be identified). It has to be noticed that if $\tau^i_1 = \tau^i_2$ in eq. (30) a classical Maxwell flow rule is recovered. Furthermore for loading cases that do not involve material rotations (tension for instance), classical Maxwell viscosity is also recovered (τ^i_2 and τ^i_1 play the same role). In contrast to this situation, shear for instance, leads to a non classical viscosity.

3.6. Modeling of Payne effect

Payne effect is macroscopically characterized by a dynamical softening. From macroscopic experiments, it is well known that this effect is strongly related to the micro-structure of the material (see Payne (1960)). Fröhlich et al. (2005), among others, studied the influence of various parameters such as the filler ratio, the surface area, the filler structure, the surface activity, etc. These parameters control the micro structure and have a direct impact on the Payne effect. An interesting discussion on the microscopic origin of the Payne effect can be found in Klüppel (2003). Earlier approaches due to Kraus and co-workers (Kraus et al. (1966)) were formulated with the idea that Payne effect is mainly a consequence of a breakage/reformation of filler to filler interaction. This model has been later enriched by many authors (see for instance Ulmer (1996)). As for the Mullins effect, there are no experimental evidences in the literature that can fully explain the origin (at the scale of the micro-structure) of the Payne effect. To the authors opinion Payne effect is a consequence of a complex micro-structural and multi-physical re-organization in aggregates of fillers due to (thermo-)mechanical loadings. In the unloaded state aggregates of fillers disseminated in rubber matrix are constituted by a filler network (physical interaction between fillers) which is surrounded by a bound rubber that could be vitreous at room temperature (see Heinrich et al. (2002); Fritzsche and Klüppel (2011)). Under dynamical mechanical loading, the physical interaction between fillers becomes weaker (as for monotonic loading) and the local temperature can increase (due to the entropic nature of rubber elasticity) leading to a rubbery state of the bound rubber. With this local softening of bound rubber and filler network breakage, occluded rubber can be released leading to a supplementary softening effect as the apparent filler

ratio will decrease. If the mechanical loading decreases or stops, a new filler network can be formed with occluded rubber. A decrease of the local temperature leads to a reformation of a rigid (vitreous) bound rubber around filler agglomerates. This scenario is one possibility among others, however it could explain the partial recovery of the Payne effect and the influence of the macroscopic temperature.

From a phenomenological point of view, Payne effect is inversely proportional to the applied amplitude and exhibits an intrinsic time (few cycles are needed to stabilize the material response when loading amplitude is increased or decreased). It can be viewed as a local damage/reforming mechanism. In the proposed model, only the damage aspect is taken into account. Furthermore it is assumed that this effect does not depends on the applied strain rate (see figure 6) the effect of the temperature is neglected (figures 5 suggest that the temperature plays a role in shear but not in tension). Using eqs. (28) and (31) in (15), it is obtained:

$$\phi^i_{payne} = -J^{-1}(g^l_i\Theta + g^c_i)(I_1(\bar{\mathbf{B}}^i_{\mathbf{e}}) - 3)\dot{\omega}_i \geq 0 \qquad i = 1..n \tag{32}$$

which is equivalent to $\dot{\omega}_i \leq 0$. It is proposed the following evolution law that fulfills the previous thermodynamical requirement:

$$\boxed{\dot{\omega}_i = -\frac{1}{h_i}\left\langle \omega_i - \left(\frac{3}{I_1(\bar{\mathbf{B}})}\right)^{r_i}\right\rangle, \quad \omega_i(t=0) = 1} \quad i = 1..n \tag{33}$$

where r_i and h_i are material parameters, h_i is homogeneous to a characteristic time for the Payne effect. In the previous expression it is made use of the previously defined Macaulay brackets. It is also assumed that these parameters do not depend on the temperature (however the apparent shear modulus is temperature dependent).

4. Material Parameters Identification and numerical results

4.1. Semi-analytical solutions for simple shear and tension

It is assumed that the deformation gradients (and the stress solution) are homogeneous and purely incompressible in the central zone of each specimen. The deformation gradients are, then, written as[4]:

$$\mathbf{F}_{tension}(t) = \begin{bmatrix} \lambda(t) & 0 & 0 \\ 0 & \frac{1}{\sqrt{\lambda(t)}} & 0 \\ 0 & 0 & \frac{1}{\sqrt{\lambda(t)}} \end{bmatrix} \qquad \mathbf{F}_{shear}(t) = \begin{bmatrix} 1 & \gamma(t) & 0 \\ 0 & 1 & 0 \\ 0 & 0 & 1 \end{bmatrix} \tag{34}$$

As $J = 1$, the constitutive relation of eq. (12) must be rewritten as[5]:

$$\boldsymbol{\sigma} = 2\rho\left(\bar{\mathbf{B}}\cdot\frac{\partial\psi_{eq}}{\partial\bar{\mathbf{B}}} + \bar{\mathbf{B}}_{\mathbf{ep}}\cdot\frac{\partial\psi_{eq}}{\partial\bar{\mathbf{B}}_{\mathbf{ep}}}\right)^{\mathrm{D}} + p\mathbf{1} + \sum_{i=1}^{n} 2\rho\left(\bar{\mathbf{B}}^i_{\mathbf{e}}\cdot\frac{\partial\psi_{vis}}{\partial\bar{\mathbf{B}}^i_{\mathbf{e}}}\right)^{\mathrm{D}} \tag{35}$$

Where p is a Lagrange multiplier (to enforce incompressibility). For simple shear, this constitutive relation can be directly used and we obtain:

$$\sigma^{shear}_{12}(t) = 2C_1(\Theta)\gamma(t) + 2C_2(\Theta)\gamma(t) + 2G_p(\Theta)\bar{B}_{ep_{12}}(t) + \sum_{i=1}^{n} 2G_i(\Theta)\omega_i(t)\bar{B}^i_{e_{12}}(t) \tag{36}$$

For uni-axial tension, the Lagrange multiplier, p, can be easily eliminated using equilibrium equation (that shows that p is homogeneous) and boundary conditions ($\sigma_{22} = \sigma_{33} = 0$). It is obtained the following

[4]Depending on the geometry (diabolo vs H2), the deformation gradient is written in Cartesian or Cylindrical coordinates.
[5]For a purely incompressible transformation, $\bar{\mathbf{F}} = \mathbf{F}$

expression:

$$\sigma_{11}^{tension}(t) = 2C_1(\Theta)\left(\lambda(t)^2 - \frac{1}{\lambda(t)}\right) + 2C_2(\Theta)\left(\lambda(t) - \frac{1}{\lambda(t)^2}\right) + 2G_p(\Theta)(\bar{B}_{ep_{11}}(t) - \bar{B}_{ep_{22}}(t)) + \sum_{i=1}^{n} 2G_i(\Theta)\omega_i(t)(\bar{B}^i_{e_{11}}(t) - \bar{B}^i_{e_{22}}(t)) \tag{37}$$

To compute expressions (36) and (37), it is required to integrate evolutions equations (22), (30) and (33). One can hardly obtain general analytical solutions to these evolution equations, therefore a numerical procedure is needed.

4.2. Numerical treatment of evolution equations

The numerical treatment of evolution equations is done numerically with the help of the NDSolve function of Mathematica (Wolfram Research (2014)). Knowing the iscochoric left Cauchy Green tensor as a function of time, the integration of the differential eq. (33) does not present any difficulty (the Macaulay brackets are replaced by the UnitStep function of Mathematica). Concerning eq. (30) the initial i^{th} differential equation is replaced by the following i^{th} differential-algebraic equations (DAE):

$$\boxed{\begin{aligned}&\dot{\bar{\mathbf{B}}}^{i}_{\mathbf{e}} = \mathbf{L}\cdot\bar{\mathbf{B}}^i_{\mathbf{e}} + \bar{\mathbf{B}}^i_{\mathbf{e}}\cdot\mathbf{L}^{\mathrm{T}} - \frac{2}{3}(\mathbf{1}:\mathbf{L})\bar{\mathbf{B}}^i_{\mathbf{e}} - \frac{1}{J\tau_1^i}\bar{\mathbf{B}}^i_{\mathbf{e}}\cdot\bar{\mathbf{B}}^{i\ \mathrm{D}}_{\mathbf{e}} \\ &\quad - \left(\frac{1}{J\tau_2^i} - \frac{1}{J\tau_1^i}\right)\sum_{a=1}^{3}(\bar{\mathbf{V}}^i_{\mathbf{e}}\cdot\mathbf{n_a})\otimes(\bar{\mathbf{V}}^i_{\mathbf{e}}\cdot\mathbf{n_a})(\mathbf{n_a}\cdot\bar{\mathbf{B}}^{i\ \mathrm{D}}_{\mathbf{e}}\cdot\mathbf{n_a}) \\ &\bar{\mathbf{B}}^i_{\mathbf{e}} = \bar{\mathbf{V}}^i_{\mathbf{e}}\cdot\bar{\mathbf{V}}^i_{\mathbf{e}} \\ &\bar{\mathbf{B}}^i_{\mathbf{e}}(t=0) = \mathbf{1}, \bar{\mathbf{V}}^i_{\mathbf{e}}(t=0) = \mathbf{1}\end{aligned}} \tag{38}$$

It is therefore considered that $\bar{\mathbf{B}}^i_{\mathbf{e}}$ and $\bar{\mathbf{V}}^i_{\mathbf{e}}$ are two independent variables to be integrated which are linked with an algebraic relation. Furthermore it is considered that the viscoelastic Cauchy Green tensor and left pure deformation tensors take the following form (for shear or tension load cases):

$$\bar{\mathbf{B}}^i_{\mathbf{e}}(t) = \begin{bmatrix} \bar{B}^i_{e_{11}}(t) & \bar{B}^i_{e_{12}}(t) & 0 \\ \bar{B}^i_{e_{12}}(t) & \bar{B}^i_{e_{22}}(t) & 0 \\ 0 & 0 & 1/(\bar{B}^i_{e_{11}}(t)\bar{B}^i_{e_{22}}(t)) \end{bmatrix}, \quad \bar{\mathbf{V}}^i_{\mathbf{e}}(t) = \begin{bmatrix} \bar{V}^i_{e_{11}}(t) & \bar{V}^i_{e_{12}}(t) & 0 \\ \bar{V}^i_{e_{12}}(t) & \bar{V}^i_{e_{22}}(t) & 0 \\ 0 & 0 & 1/(\bar{V}^i_{e_{11}}(t)\bar{V}^i_{e_{22}}(t)) \end{bmatrix} \tag{39}$$

For shear and tension, the principal directions of the isochoric left Cauchy Green tensor ($n_a(t)$) can be analytically expressed as functions of time and the tensorial DAE, eq (38), is replaced by a DAE system with 6 unknowns ($\bar{B}^i_{e_{11}}(t)$, $\bar{B}^i_{e_{22}}(t)$, $\bar{B}^i_{e_{12}}(t)$, $\bar{V}^i_{e_{11}}(t)$, $\bar{V}^i_{e_{22}}(t)$, $\bar{V}^i_{e_{12}}(t)$). It can be remarked that the DAE system depends only on the material parameters τ_1^i and τ_2^i. If this material parameters are known (a priori), the differential system can be integrated independently from other material parameters.

The integration of eq. (22), is based on the same analytical form for $\bar{\mathbf{B}}_{\mathbf{ep}}$:

$$\bar{\mathbf{B}}_{\mathbf{ep}}(t) = \begin{bmatrix} \bar{B}_{ep_{11}}(t) & \bar{B}_{ep_{12}}(t) & 0 \\ \bar{B}_{ep_{12}}(t) & \bar{B}_{ep_{22}}(t) & 0 \\ 0 & 0 & 1/(\bar{B}_{ep_{11}}(t)\bar{B}_{ep_{22}}(t)) \end{bmatrix} \tag{40}$$

Introducing (40) in eq. (22), it is obtained a system of differential equations with three unknowns ($\bar{B}_{ep_{11}}(t)$, $\bar{B}_{ep_{22}}(t)$, $\bar{B}_{ep_{12}}(t)$). As previously, the Macaulay brackets are replaced by the UnitStep function of Mathematica.

1. Equilibrium contribution, minimize $Err_{eq}(C_1, C_2, G_p, \chi, \zeta)$ such that:

$$Err_{eq} = \sum_{j=1}^{N_{temperature}} \left((\frac{1}{N_{points}^{tension}}) \sum_{i=1}^{N_{points}^{tension}} \frac{(\boldsymbol{\sigma}_{exp_{11}}^{i,j} - \boldsymbol{\sigma}_{eq_{11}}^{i,j})^2}{Max(\boldsymbol{\sigma}_{exp_{11}}^{i,j})^2} + (\frac{1}{N_{points}^{shear}}) \sum_{i=1}^{N_{points}^{shear}} \frac{(\boldsymbol{\sigma}_{exp_{12}}^{i,j} - \boldsymbol{\sigma}_{eq_{12}}^{i,j})^2}{Max(\boldsymbol{\sigma}_{exp_{12}}^{i,j})^2} \right)$$

   where $\boldsymbol{\sigma}_{exp_{11}}^{i,j}$, $\boldsymbol{\sigma}_{exp_{12}}^{i,j}$ and $\boldsymbol{\sigma}_{eq_{11}}^{i,j}$, $\boldsymbol{\sigma}_{eq_{12}}^{i,j}$ denote the components of respectively the experimental and the model equilibrium Cauchy stress obtained in tension or shear for a strain amplitude i and at a temperature Θ_j. The aforementioned minimization is done under the constraints: $C_1(\Theta) \geq 0$, $C_2(\Theta) \geq 0$, $G_p(\Theta) \geq 0$, $\chi(\Theta) \geq 0$, $\zeta(\Theta) \geq 0$ $\forall \Theta \in [230K, 350K]$. For this step, we use the experimental data presented in figures 3(c) and 3(d)
2. Fixing a range of characteristic times τ_1^i, τ_2^i and Payne parameters h_i, r_i with the constraint $\tau_1^i \geq \tau_2^i$. Typically with $\tau_1, \tau_2 \in [10^{-4}, 10^{-3}, 10^{-2}, 10^{-1}, 1, 10, 10^2, 10^3]$, $h \in [10^{-1}]$, $r \in [1, 10]$ there are 72 admissible combinations (this set was used for the present identification).
3. Pre-computing the solution of viscous flow (eq. (30)) and Payne evolution (eq. (33)) for each temperature and each combination of frequency and amplitude of cyclic dynamical experiments in shear and tension and each of the 72 admissible combinations of material parameters.
4. For each temperature (independently from each other), minimize $Err_{neq}(G_1, G_2, .., G_n)$ such that:

$$Err_{neq}(G_1, G_2, .., G_n) = \sum_{j=1}^{N_{cyclictests}} \frac{(R_{exp}^j - R^j)^2}{{R_{exp}^j}^2} + \sum_{j=1}^{N_{cyclictests}} \frac{(D_{exp}^j - D^j)^2}{{D_{exp}^j}^2}$$

   where R_{exp}^j and R^j are respectively the experimental and the model dynamical stiffness (slope of the median of the hysteresis), D_{exp}^j and D^j denotes respectively the experimental and the model hysteresis area (for a stabilized cycle). As evolution equations has been pre-determined at step 3, the D^j and R^j are only dependent on G_i. Mathematica is used to obtain an analytic expression of these functions and the minimization becomes a simple constrained minimization problems (the conditions $G_i \geq 0 \, \forall i$ are imposed). In this step, the experimental data from dynamical shear tests (f=3Hz,6Hz,12Hz,25Hz and A=100%,50%,25%,10%) and from dynamical tension tests (f=3Hz,12Hz and A=25%,10%) are used.
5. Selecting the most significant characteristic times. For each temperature it can be selected the most significant parameters $(\tau_1^i, \tau_2^i, h_i, r_i)$ by computing Err_{neq} with previously obtained G_i excepted the k^{th} combination for which G_k is imposed to be null. If Err_{neq} is not sensitive to the removal of the k^{th} combination, this combination is removed from the initial list. A common (to each temperature) reduced list of characteristic times is then obtained.
6. The final identification is run by minimizing $Err(g_1^l, g_1^c, g_2^l, g_2^c, .., g_n^l, g_n^c)$, where:

$$Err(g_1^l, g_1^c, g_2^l, g_2^c, .., g_n^l, g_n^c) = \sum_{j=1}^{N_{temperature}} Err_{neq}(g_1^l \Theta_j + g_1^c, .., g_n^l \Theta_j + g_n^c)$$

   As for the first step this minimization is done under the constraints $g_i^l \Theta_j + g_i^c \geq 0 \, \forall i, \Theta \in [230K, 350K]$. The same experimental data than for the step 4, are used in this final step.

Table 2: Identification of material parameters

4.3. Identification of material parameters

The material parameters identification shares the same concepts as those exposed in Delattre et al. (2014). Basically, the identification is done at each temperature separately to determine the evolution of the material parameters upon temperature. Once this evolution is chosen (linear for this model) material parameters are

re-identified taking into account all the temperatures simultaneously. The material identification procedure can be decomposed in six steps: first the equilibrium contribution is determined (parameters $C_1, C_2, G_p, \chi, \zeta$) and the obtained parameters are kept fixed. For this step, it is used the experimental data obtained from relaxation tests (figures 3(c) and 3(d)) and the objective function is based on a classical square root distance of experimental and semi-analytical values.

In a second step, a set of characteristic times (τ_1^1,τ_2^1, τ_1^2,τ_2^2, .., τ_1^n,τ_2^n) and Payne parameters (h_1, r_1, h_2, r_2, .., h_n, r_n) are arbitrarily fixed. This allows to integrate each evolution equation for each test case separately and it can be obtained a semi-analytical expression of the identification error. The associated shear moduli ($G_1, G_2, .., G_n$) are then identified in a fourth step for each temperature separately. In this paper, we consider an original identification error: rather than a classical error measure (mean square distance between the experimental points and model predictions), the present error is based on the difference between the hysteresis area and the dynamic modulus obtained from experiments and model. The arbitrary set of characteristic times and Payne parameters is eventually redefined in a fifth step to keep only the more significant G_i (and therefore to eliminate non significant characteristic times). Finally in the last step, the temperature evolution of the shear modulus G_i is obtained. The procedure allows to let the minimization process determine the number of characteristic times that are needed to represent the behavior. The identification procedure is summed up in the table 2.

Obviously, the identification procedure is sensitive to the a priori chosen set of characteristic times and Payne parameters. Nevertheless, this strategy exhibits a total computational cost which is several order of magnitude lower com Pared to a frontal identification strategy for which only the number of viscous phenomena is given and all the material parameters are unknown a priori. This is due to the fact that nonlinear complex flow rules (viscosity and Payne) can be pre-integrated for each test case (temperature, frequency, amplitude). Furthermore, the final number of characteristic times, n, is optimized by the procedure.

Finally the results obtained at the end of the identification process are given in the table 3. It is interesting to note that the result of the identification is a priori compatible with the hypothesis of an entropic elasticity like response of the equilibrium part of the model (parameters C_1, C_2, G_p). Concerning the viscous contribution, the identification process gives less clear results as the temperature dependency can be either increasing or decreasing. Furthermore, starting from 72 possible combinations of viscous parameters, the identification process has retained in the end only 7 contributions. Looking at the parameters τ_1^i and τ_2^i there are only 2 contributions for which the response is selected by the identification process as purely isotropic (i.e $\tau_1 = \tau_2$).

4.4. Identification results: comparison of experimental and model responses

In this section, we focus only on the identification results and the capacity of the model to correctly describe the experimental data that were used for the identification process. Figures 11 show a comparison between the model and experimental response for the equilibrium hysteresis at different temperatures. It can

C_1 (MPa)	C_2 (MPa)	G_p (MPa)	χ (MPa)	ζ (MPa.s)
0.	$9.6e^{-4}\theta + 3.8e^{-2}$	$5.3e^{-4}\theta + 2.8e^{-1}$	$4.1e^{-3}\theta + 1.9e^{-1}$	$4.0e^{3}\theta + 1.4e^{6}$
τ_1^i (s)	τ_2^i (s)	h^i (s)	r^i	G_i (MPa)
$1.e^{-2}$	$1.e^{-4}$	$1.5e^{-1}$	1.	$2.7e^{-3}\theta + 1.7e^{-1}$
1.	$1.e^{-2}$	$1.5e^{-1}$	1.	$-1.2e^{-3}\theta + 8.6e^{-2}$
1.	1.	$1.5e^{-1}$	1.	$-2.7e^{-3}\theta + 2.6e^{-1}$
$1.e^{2}$	$1.e^{-2}$	$1.5e^{-1}$	1.	$3.0e^{-4}\theta + 1.3e^{-2}$
$1.e^{3}$	$1.e^{-2}$	$1.5e^{-1}$	1.	$3.3e^{-4}\theta + 1.1e^{-1}$
$1.e^{3}$	$1.e^{-1}$	$1.5e^{-1}$	1.	$-2.6e^{-5}\theta + 1.4e^{-1}$
$1.e^{3}$	$1.e^{3}$	$1.5e^{-1}$	10.	$-4.9e^{-5}\theta + 1.8e^{-1}$

Table 3: Final identification results (it has been used the notation: $\theta = \Theta - 273$)

be seen that both responses are in good accordance even if the non linearity in shear for large deformation is not well captured by the model. Thermal stiffening (entropic behavior) and hysteresis area decreasing upon temperature increase are correctly described.

The dynamic response without preload (null mean stress) is illustrated at figures 12 and 13. First it can be remarked that the Payne effect is well captured by the model: small and large hysteresis are correctly described both in tension and shear. Furthermore the temperature dependance of the Payne effect is also well described even if the material parameters that control the evolution of the ω_i are not temperature dependent. As for the equilibrium hysteresis the non-linearity of the dynamic response in shear for large strain is not perfectly represented (particularly for $\theta = -40^oC$). Focusing on the frequency dependency, the results are in very good agreement in the range 3Hz to 12Hz both for shear and tension and for each temperature (idem for 25Hz in shear, see figures 14). If one look at a smaller rate of loading (not used in the identification), the results illustrate that the model has a faster decrease of the hysteresis area and therefore the long time viscosity is not fully described (see figures 15). It can also be remarked that this long time viscosity is not embedded in the equilibrium hysteresis response which is here correctly described.

4.5. Preliminary validation: influence of the preload

As a preliminary validation of the model, we propose to compare model and experimental results in the case of dynamical tests with preload at different temperatures (both in shear and tension). These tests were not used in the identification process. Figures 16 show that it is obtained a very good agreement (exception

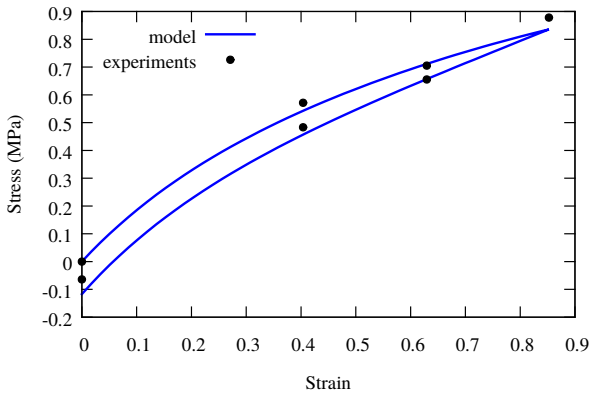

(a) Tension at $\theta = -40^oC$

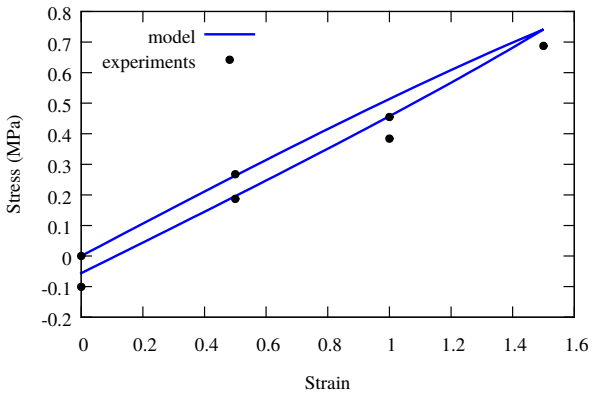

(b) Simple Shear at $\theta = -40^oC$

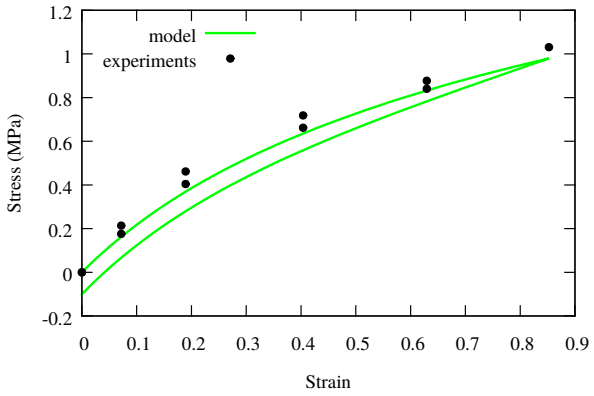

(c) Tension at $\theta = 20^oC$

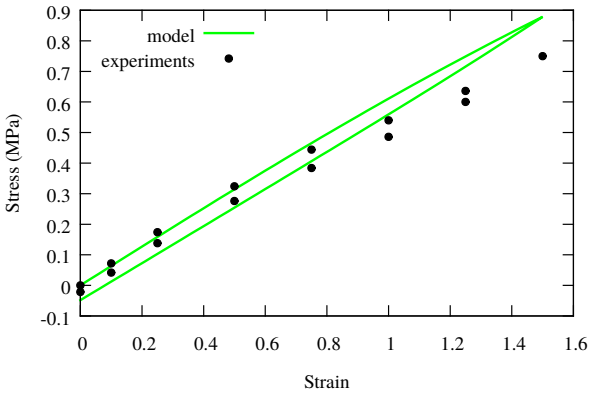

(d) Simple Shear at $\theta = 20^oC$

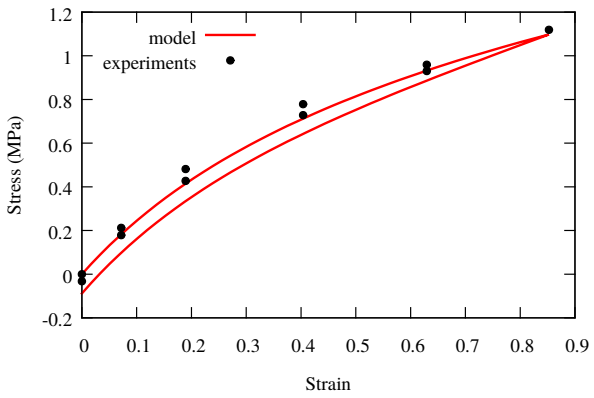

(e) Tension at $\theta = 70^oC$

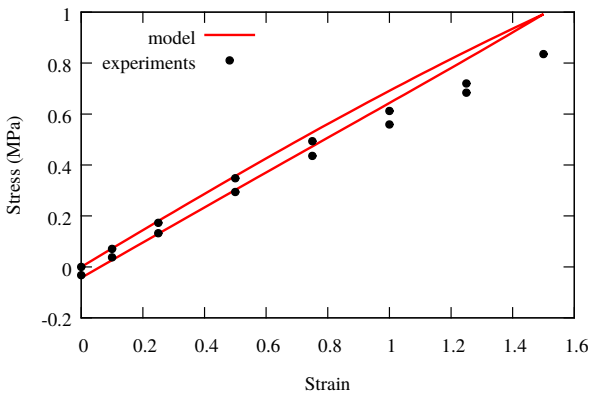

(f) Simple Shear at $\theta = 70^oC$

Figure 11: Identification results for the equilibrium hysteresis

made of the Tension/Compression at $\theta = -40C$) between experimental and numerical data. The influence of the preload on the Payne effect seems correctly described for shear. As observed experimentally, the preload has a stronger influence in uniaxial tension than in simple shear. Therefore, the induced anisotropic viscous flows allow to capture this asymmetric behavior, which could have a strong influence in practical applications (i.e., for more complex loading).

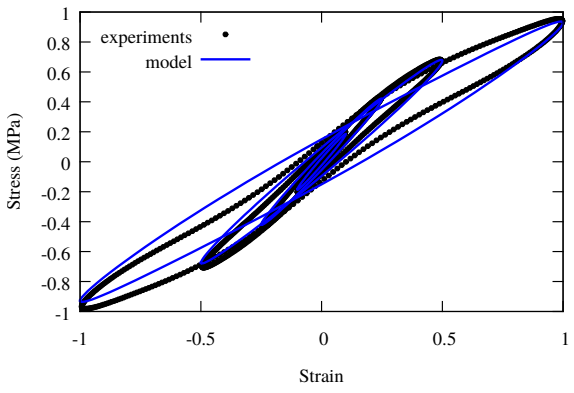

(a) Simple shear at $f = 3Hz, \theta = -40^oC$

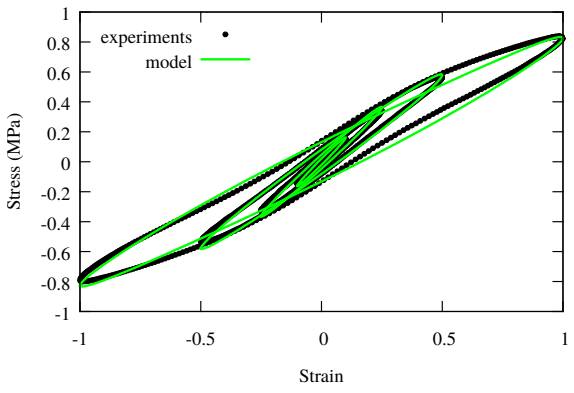

(b) Simple shear at $f = 3Hz, \theta = 20^oC$

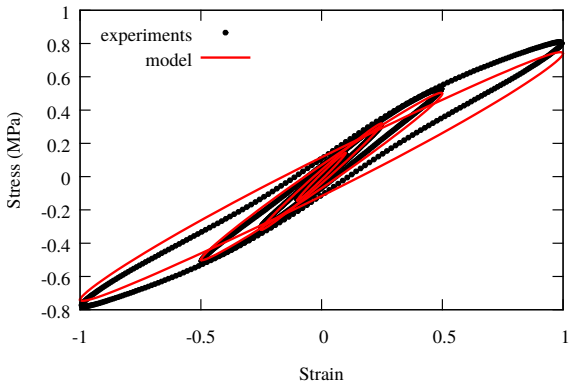

(c) Simple shear at $f = 3Hz, \theta = 70^oC$

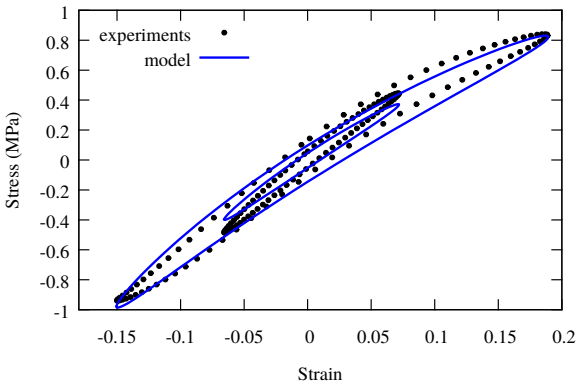

(d) Tension/Compression at $f = 3Hz, \theta = -40^oC$

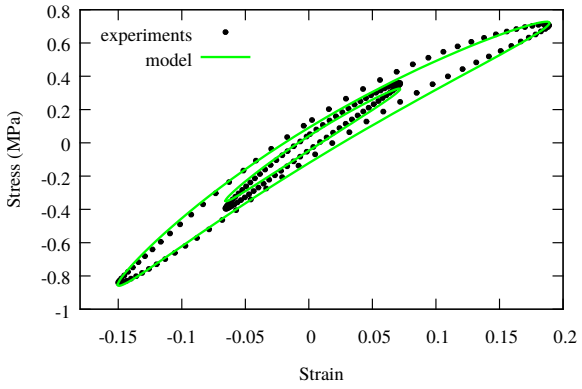

(e) Tension/Compression at $f = 3Hz, \theta = 20^oC$

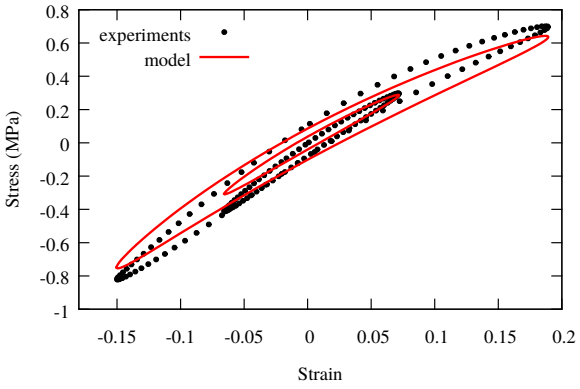

(f) Tension/Compression at $f = 3Hz, \theta = 70^oC$

Figure 12: Identification results for cyclic sinusoidal dynamic test at $f = 3Hz$ (only the stabilized response is plotted)

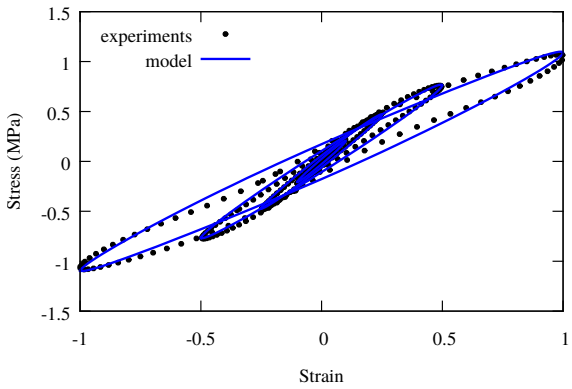

(a) Simple shear at $f = 12Hz, \theta = -40^oC$

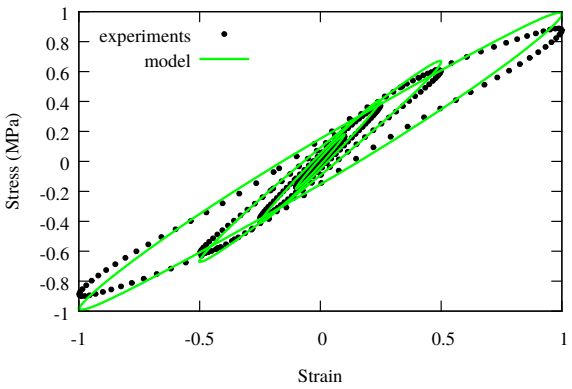

(b) Simple shear at $f = 12Hz, \theta = 20^oC$

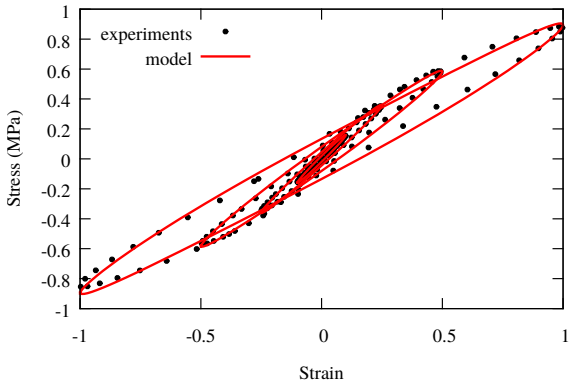

(c) Simple shear at $f = 12Hz, \theta = 70^oC$

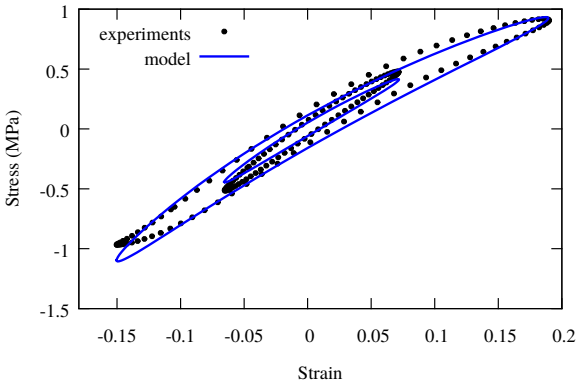

(d) Tension/Compression at $f = 12Hz, \theta = -40^oC$

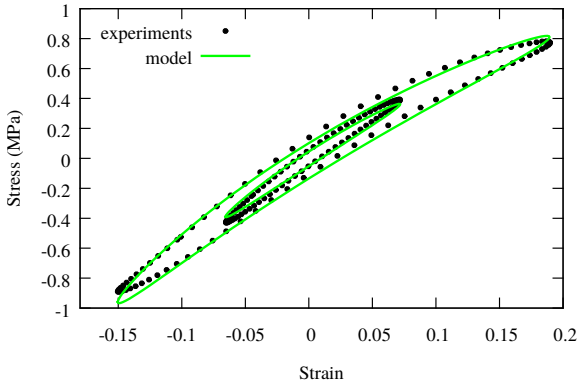

(e) Tension/Compression at $f = 12Hz, \theta = 20^oC$

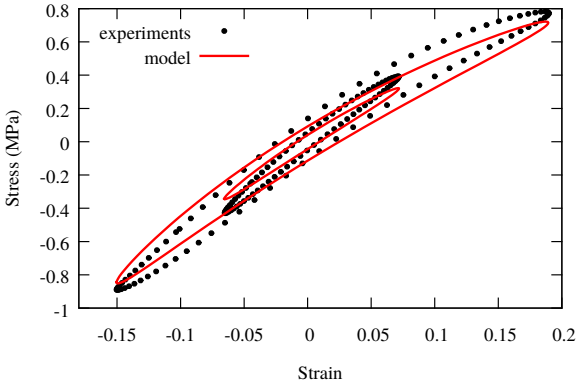

(f) Tension/Compression at $f = 12Hz, \theta = 70^oC$

Figure 13: Identification results for cyclic sinusoidal dynamic test at $f = 12Hz$ (only the stabilized response is plotted)

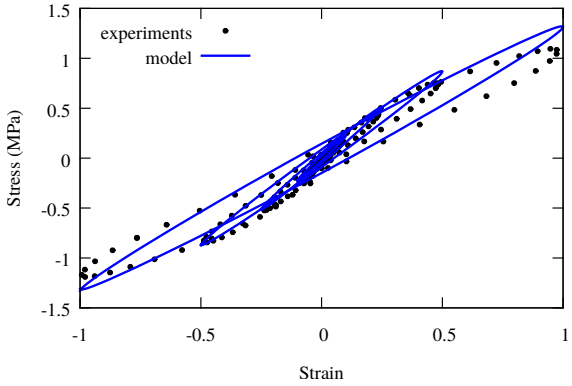

(a) Simple shear at $f = 25Hz, \theta = -40^oC$

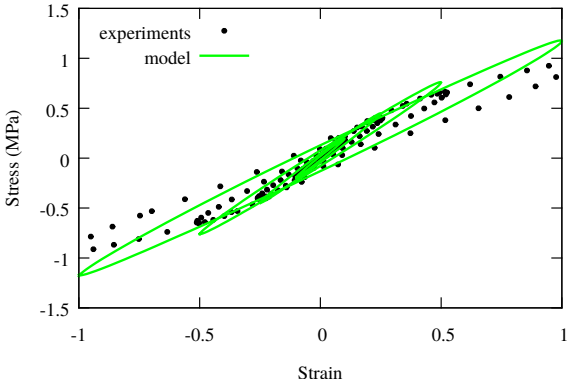

(b) Simple shear at $f = 25Hz, \theta = 20^oC$

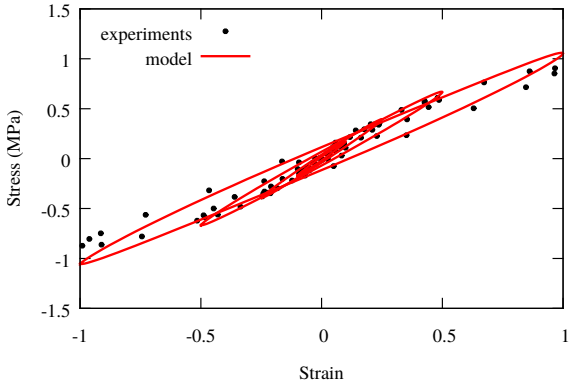

(c) Simple shear at $f = 25Hz, \theta = 70^oC$

Figure 14: Identification results for cyclic sinusoidal dynamic test at $f = 25Hz$ (only the stabilized response is plotted)

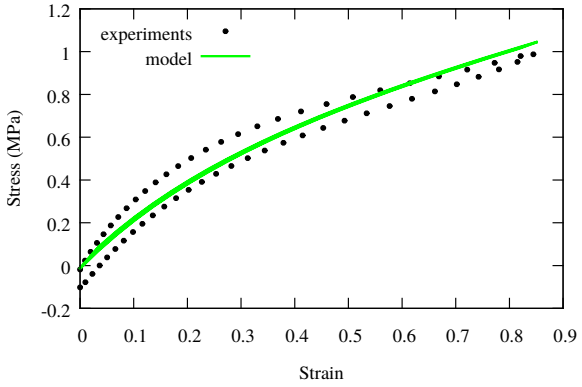

(a) Simple shear at $\theta = 20^oC$

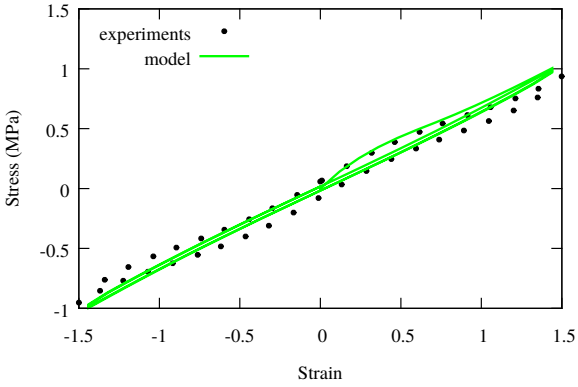

(b) Tension at $\theta = 20^oC$

Figure 15: CoMParison experiment/model for cyclic triangular dynamic test at $f = 0.01Hz$

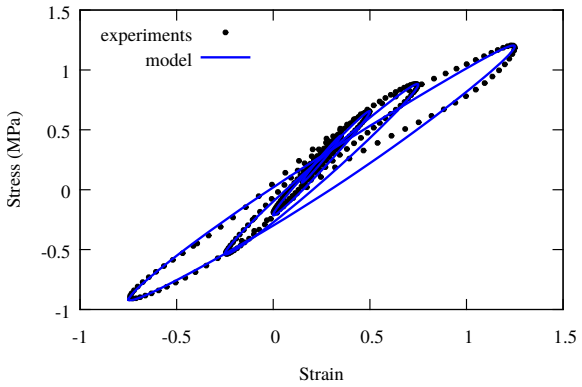

(a) Simple shear at $f = 12Hz, \theta = -40^oC$

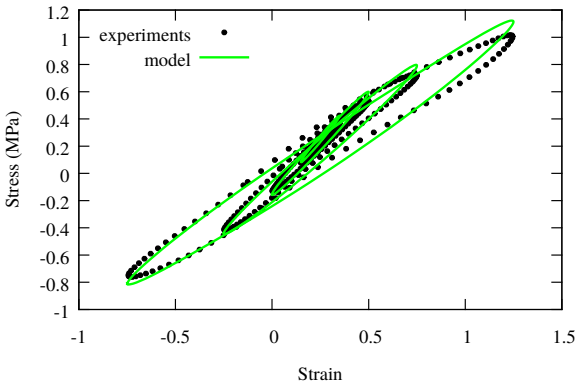

(b) Simple shear at $f = 12Hz, \theta = 20^oC$

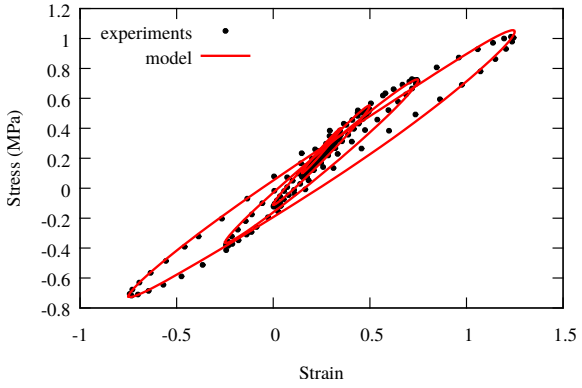

(c) Simple shear at $f = 12Hz, \theta = 70^oC$

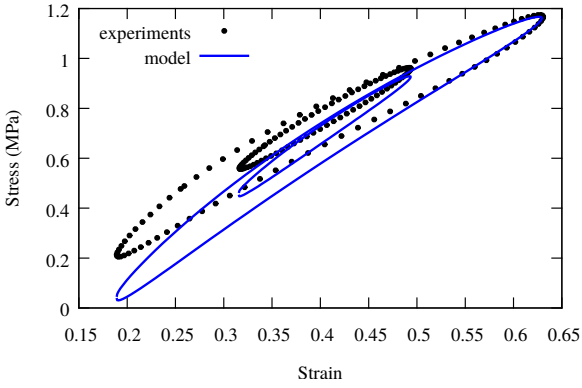

(d) Tension/Compression at $f = 12Hz, \theta = -40^oC$

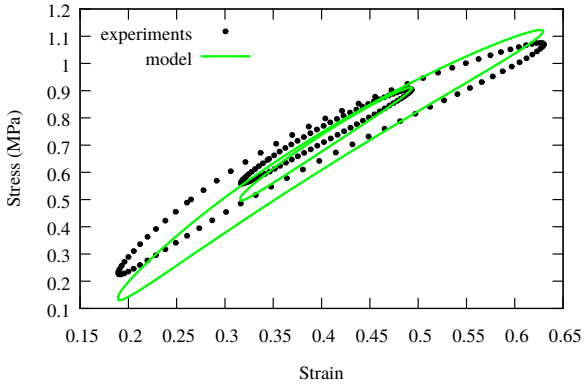

(e) Tension/Compression at $f = 12Hz, \theta = 20^oC$

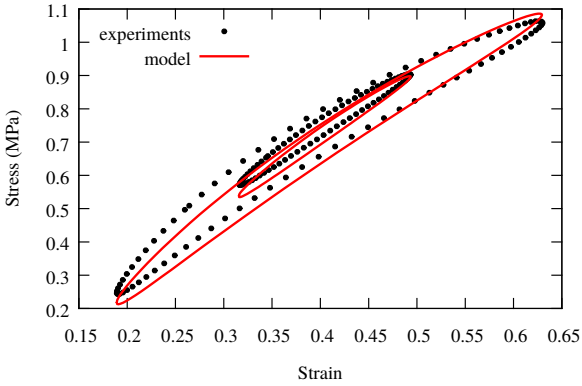

(f) Tension/Compression at $f = 12Hz, \theta = 70^oC$

Figure 16: CoMParison experiment/model for cyclic sinusoidal dynamic test with preload at $f = 12Hz$ (only the stabilized response is plotted)

5. Conclusion

In this work, we have proposed a new constitutive model for finite rubber viscoelasticity which takes into account of specific phenomena exhibited by filled rubber submitted to dynamical loading at various temperatures. First the introduction of directional viscous flows has permitted to correctly represent the multi-axial behavior and particularly the specific dependency of the dynamical response on preload. We have adopted the classical idea of a representation of a continuum spectrum of relaxation with a combination of discrete viscous stresses. The number of viscous stresses is automatically determined by a specific developed material fitting procedure. In the present case 7 viscous stresses are needed to represent the behavior in a range of frequency and temperatures that corresponds to the industrial application. To describe the Payne effect, we have proposed a new model based on the introduction of internal variables that affect the apparent modulus of each viscous stresses. The evolution equations, associated to these variables, take into account of the maximum strain energy seen by the material through the first invariant of the left Cauchy Green tensor. The introduction of both a characteristic time for Payne effect and a yield function in the evolution equation allows to cover a wide range of dynamical amplitudes (from 5% to 150%).

Com Pared to previous approaches the present model seems very promising as it seems valuable to cover a wide range of dynamical frequencies, amplitudes and temperatures in a multi-axial context. Nevertheless this work needs to be completed with the introduction of new mechanisms to describe the partial recoverability of the Payne effect.

To proceed further and to validate the proposed model, we need to do a rigorous comparison of model and experimental responses in non homogeneous and multi-axial test cases. This will require a finite element implementation and a consistent linearization. This work has been done and will be presented in a future publication. Concerning multi-axial experiments, we will provide validation of the model on tension/torsion or compression /torsion tests on the diabolo specimen but we will also propose a comparison on dynamical shear test on laminated bearing under static compression (see figure 17). Digital image correlation results will permit to provide a local comparison of finite elements and experimental data.

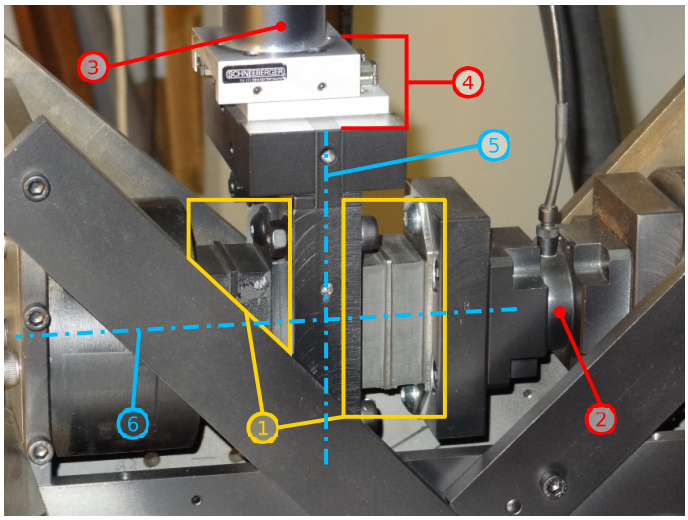

Figure 17: laminated bearing setup for dynamical shear test with static compression.

6. Acknowledgments

The authors gratefully thank Professor Philippe Pilvin for interesting discussions about induced anisotropy which has led to the present developments. This work has received a financial support of Airbus Helicopters,

this support is also gratefully acknowledged.

References

Bergström, J., Boyce, M., 2000. Large strain time-dependent behavior of filled elastomers. Mechanics of Materials 32 (11), 627 – 644.
URL http://www.sciencedirect.com/science/article/pii/S0167663600000284

Coleman, B. D., Noll, W., Apr 1961. Foundations of linear viscoelasticity. Rev. Mod. Phys. 33, 239–249.
URL http://link.aps.org/doi/10.1103/RevModPhys.33.239

Delattre, A., Lejeunes, S., Méo, S., Lacroix, F., Richard, C., 2014. On the multiaxial amplitude and frequency dependent behavior of rubber: experiments and constitutive modeling. Rubber Chemistry and Technology 87 (3), 557–578.
URL https://hal.archives-ouvertes.fr/hal-01057026

Flory, R. J., 1961. Thermodynamic relations for highly elastic materials. Transactions of the Faraday Society 57, 829–838.

Fritzsche, J., Klüppel, M., 2011. Structural dynamics and interfacial properties of filler-reinforced elastomers. Journal of Physics: Condensed Matter 23 (3), 035104.
URL http://stacks.iop.org/0953-8984/23/i=3/a=035104

Fröhlich, J., Niedermeier, W., Luginsland, H.-D., 2005. The effect of fillerfiller and fillerelastomer interaction on rubber reinforcement. Composites Part A: Applied Science and Manufacturing 36 (4), 449 – 460, filled and Nano-Composite Polymer Materials.
URL http://www.sciencedirect.com/science/article/pii/S1359835X04002428

Germain, P., Nguyen, Q., Suquet, P., 1983. Continuum thermodynamics. Journal of Applied Mechanics 50, 1010–1020.
URL http://dx.doi.org/10.1115/1.3167184

Heinrich, G., Klüppel, M., Vilgis, T. A., 2002. Reinforcement of elastomers. Current Opinion in Solid State and Materials Science 6 (3), 195 – 203.
URL http://www.sciencedirect.com/science/article/pii/S135902860200030X

Klüppel, M., 2003. The role of disorder in filler reinforcement of elastomers on various length scales. In: Capella, B., Geuss, M., Klüppel, M., Munz, M., Schulz, E., Sturm, H. (Eds.), Filler-Reinforced Elastomers/Sanning Force Microscopy. Vol. 164 of Advances in Polymer Science. Springer Berlin Heidelberg, pp. 1–86.
URL http://dx.doi.org/10.1007/b11054

Kraus, G., Childers, C. W., Rollmann, K. W., 1966. Stress softening in carbon black reinforced vulcanizates. strain rate and temperature effects. Rubber Chemistry and Technology 39 (5), 1530–1543.
URL http://dx.doi.org/10.5254/1.3547068

Linder, C., Tkachuk, M., Miehe, C., 2011. A micromechanically motivated diffusion-based transient network model and its incorporation into finite rubber viscoelasticity. Journal of the Mechanics and Physics of Solids 59 (10), 2134 – 2156.
URL http://www.sciencedirect.com/science/article/pii/S0022509611001086

Lion, A., 1996. A constitutive model for carbon black filled rubber: Experimental investigations and mathematical representation. Continuum Mechanics and Thermodynamics 8 (3), 153–169.
URL http://dx.doi.org/10.1007/BF01181853

Lion, A., Kardelky, C., 2004. The payne effect in finite viscoelasticity: constitutive modelling based on fractional derivatives and intrinsic time scales. International Journal of Plasticity 20 (7), 1313 – 1345.
URL http://www.sciencedirect.com/science/article/pii/S0749641903001360

Martinez, J., Boukamel, A., Méo, S., Lejeunes, S., 2011. Statistical approach for a hyper-visco-plastic model for filled rubber: Experimental characterization and numerical modeling. European Journal of Mechanics - A/Solids 30 (6), 1028 – 1039.
URL http://www.sciencedirect.com/science/article/pii/S0997753811000982

Meo, S., Boukamel, A., Debordes, O., 2002. Analysis of a thermoviscoelastic model in large strain. Computers & Structures 80 (2730), 2085 – 2098.
URL http://www.sciencedirect.com/science/article/pii/S0045794902002468

Miehe, C., Göktepe, S., 2005. A micromacro approach to rubber-like materials. part ii: The micro-sphere model of finite rubber viscoelasticity. Journal of the Mechanics and Physics of Solids 53 (10), 2231 – 2258.
URL http://www.sciencedirect.com/science/article/pii/S0022509605000918

Morman, K.N., J., 1988. An adaptation of finite linear viscoelasticity theory for rubber-like viscoelasticity by use of a generalized strain measure. Rheologica Acta 27 (1), 3–14.
URL http://dx.doi.org/10.1007/BF01372444

Omnès, B., Thuillier, S., Pilvin, P., Grohens, Y., Gillet, S., 2008. Effective properties of carbon black filled natural rubber: Experiments and modeling. Composites Part A: Applied Science and Manufacturing 39 (7), 1141 – 1149.
URL http://www.sciencedirect.com/science/article/pii/S1359835X08001097

Payne, A. R., 1960. A note on the existence of a yield point in the dynamic modulus of loaded vulcanizates. Journal of Applied Polymer Science 3 (7), 127–127.
URL http://dx.doi.org/10.1002/app.1960.070030721

Reese, S., 2003. A micromechanically motivated material model for the thermo-viscoelastic material behaviour of rubber-like polymers. International Journal of Plasticity 19 (7), 909 – 940.
URL http://www.sciencedirect.com/science/article/pii/S0749641902000864

Reese, S., Govindjee, S., 1997. Theoretical and numerical aspects in the thermo-viscoelastic material behaviour of rubber-like

polymers. Mechanics of Time-Dependent Materials 1, 357–396.
URL http://dx.doi.org/10.1023/A:1009795431265

Rendek, M., Lion, A., 2010. Amplitude dependence of filler-reinforced rubber: Experiments, constitutive modelling and {FEM} implementation. International Journal of Solids and Structures 47 (21), 2918 – 2936.
URL http://www.sciencedirect.com/science/article/pii/S0020768310002428

Ulmer, J. D., 1996. Strain dependence of dynamic mechanical properties of carbon black-filled rubber compounds. Rubber Chemistry and Technology 69 (1), 15–47.
URL http://dx.doi.org/10.5254/1.3538354

Wolfram Research, I., 2014. Mathematica.

Wollscheid, D., Lion, A., 2014. The benefit of fractional derivatives in modelling the dynamics of filler-reinforced rubber under large strains: a comparison with the maxwell-element approach. Computational Mechanics 53 (5), 1015–1031.
URL http://dx.doi.org/10.1007/s00466-013-0946-4